SUPPLEMENTARY INFORMATION

Computational design of an amidase by combining the best electrostatic features of two promiscuous hydrolases.

Miquel À. Galmés,[1] Alexander R Nödling,[2] Kaining He,[2] Louis Luk,[2,*] Katarzyna Świderek,[3,*] Vicent Moliner[1,*]

1. BioComp Group, Institute of Advanced Materials (INAM), Universitat Jaume I, 12071 Castellón, Spain.
2. School of Chemistry, Cardiff University, Main Building, Park Pl, Cardiff CF10 3AT (United Kingdom)
3. Department of Physical and Analytical Chemistry, Universitat Jaume I, 12071 Castellón, Spain.

corresponding authors:

L. Luk: lukly@cardiff.ac.uk;

K. Świderek: swiderek@uji.es;

V. Moliner: moliner@uji.es

RESULTS AND ANALYSIS

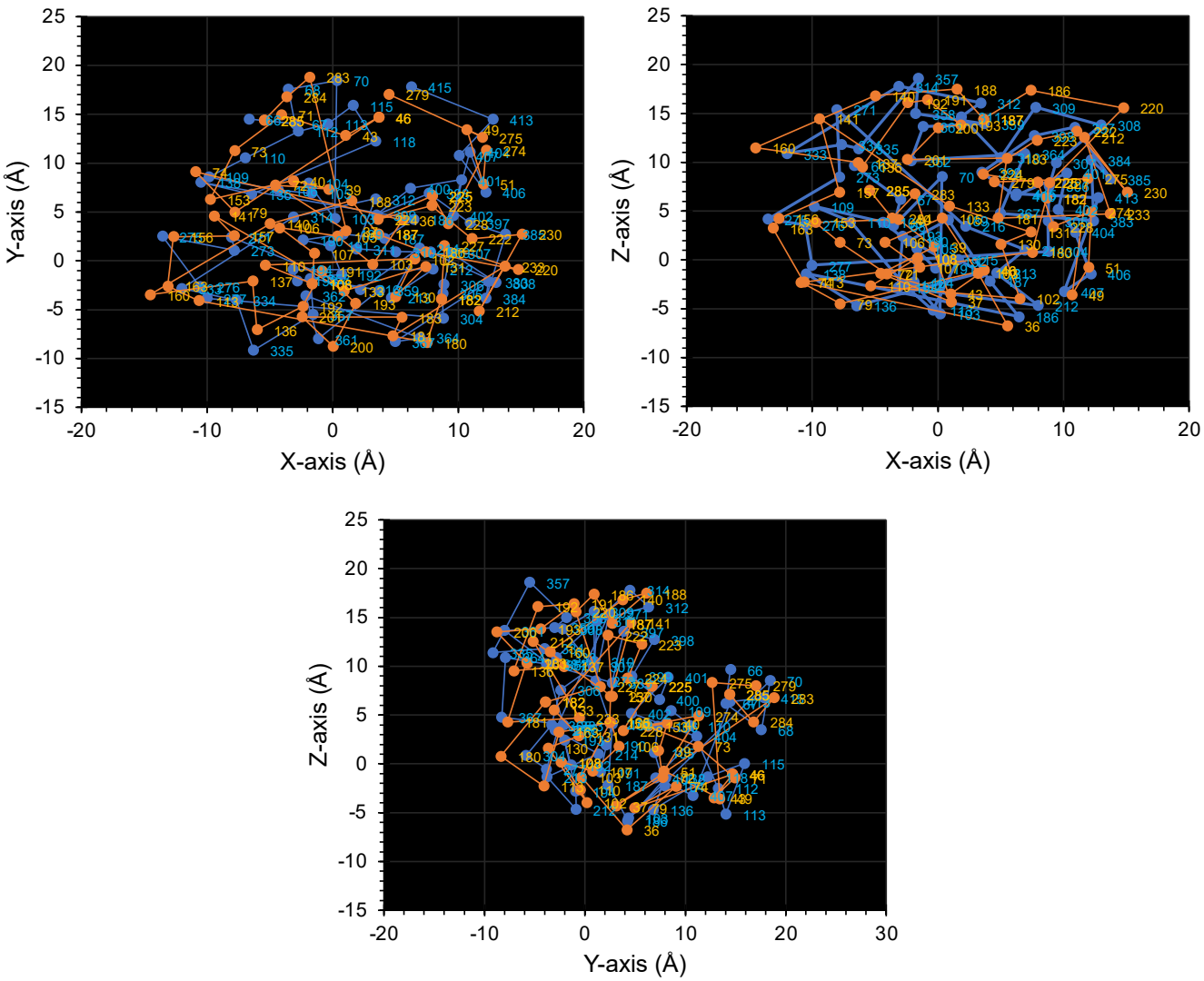

Figure S1. Overlapped centers of masses of paired residues from Bs2 (in blue) and CALB (in orange) in 3-dimensional space.

Bs2	66	67	68	70	103	104	105	106	109	110	112	113	115	118	136
	ASP	LEU	LEU	LEU	ILE	HIS	GLY	GLY	TYR	LEU	ALA	GLY	GLU	TYR	TYR
	−	|	|	|	|	+	||	.	.	||	:	.	−	.	.
	ILE	ILE	ALA	ALA	VAL	MET	GLY	THR	SER	LEU	PHE	THR	GLN	GLN	ASN
CALB	285	285	284	283	37	72	39	40	153	73	71	43	46	46	79

Bs2	138	186	187	**189**	190	191	192	193	194	212	213	214	216	271	273
	LEU	PHE	GLY	**SER**	ALA	GLY	GLY	MET	SER	ILE	MET	GLU	GLY	PHE	LEU
	.	:	.	||	.	||	||	|	.	|	|	−	.	:	.
	ASN	LEU	THR	**SER**	GLN	GLY	GLY	GLY	VAL	LEU	ALA	PHE	PRO	ALA	GLN
CALB	74	36	103	**105**	106	107	108	108	110	102	130	131	133	141	157

Bs2	275	276	277	304	305	306	307	308	309	**310**	311	312	314	333	334
	PHE	GLN	PRO	ILE	GLY	THR	THR	ARG	ASP	**GLU**	GLY	TYR	PHE	TYR	LEU
	.	.	o	.	|	.	|	+	−	|	−	−	:	:	|
	GLN	LEU	TRP	THR	LEU	LEU	SER	PHE	THR	**ASP**	ASP	GLU	LEU	GLY	GLY
CALB	156	163	113	180	182	182	227	220	186	**187**	187	188	140	160	137

Bs2	335	357	358	359	361	362	364	367	383	384	385	397	398	**399**	400
	LEU	MET	MET	THR	LEU	LEU	TRP	ALA	TYR	ARG	PHE	ALA	PHE	**HIS**	ALA
	+	.	.	|	−	.	|	.	.	+	.	|	−	||	||
	LYS	PRO	GLN	GLN	ASP	SER	TYR	ASN	SER	ALA	SER	ILE	ASP	**HIS**	ALA
CALB	136	192	191	193	200	201	183	181	233	212	230	222	223	**224**	225

Bs2	401	402	404	406	407	413	415
	LEU	GLU	PRO	VAL	PHE	LEU	ARG
	|	−	.	.	−	|	+
	ALA	LEU	ALA	ASN	ASP	ALA	ALA
CALB	225	228	274	51	49	275	279

Figure S2. Structural alignment of Bs2 and CALB. In red the paired residues of the catalytic triad are highlighted. Double "| |" is used to mark equal residues; single "|" refers to a change to a residue of the same family (polar, non-polar, positively charged, negatively charged, and aromatic); colon ":" is marking the change between non-polar to aromatic; simple dot "." refers to the change between polar and non-polar residues; "o" is used for the changes among polar and aromatic residues; "+" refers to the change in a positively charged residue; and "-" refers to a change in a negatively charged residue.

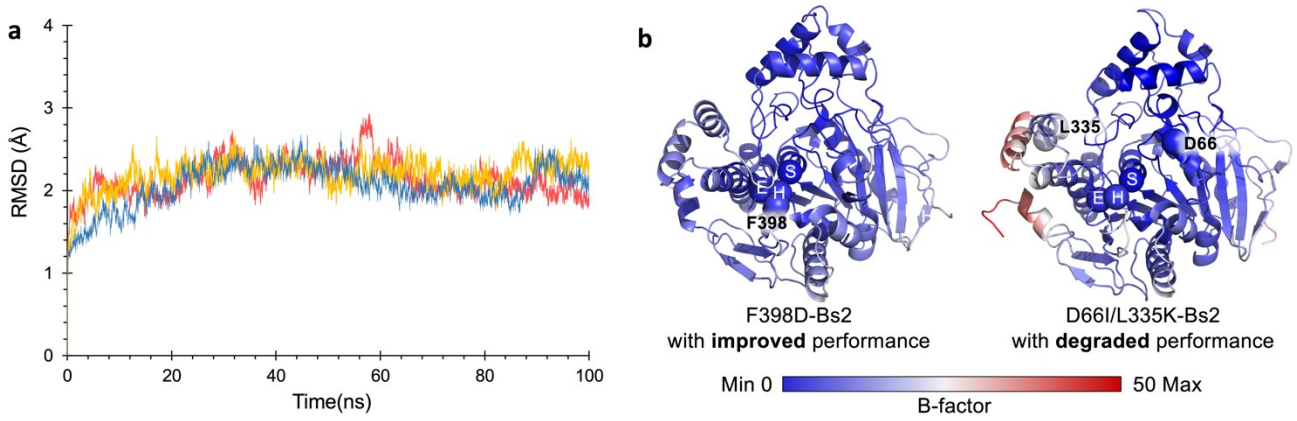

Figure S3. Analysis of 100 ns molecular dynamic simulations. a, Root mean square deviation (RMSD) of the position of Cα, C, and N atoms of the backbone along 100 ns of MD simulations computed for the F398D Bs2 variant (blue), F398D-H^+ Bs2 variant (yellow) and D66I/L335K Bs2 variant (red) along MD simulations. **b,** B-factor per atom computed as atomic oscillations around the equilibrium positions recorded during MD simulations. The red regions correspond to the flexible parts of the protein, the blue areas are static.

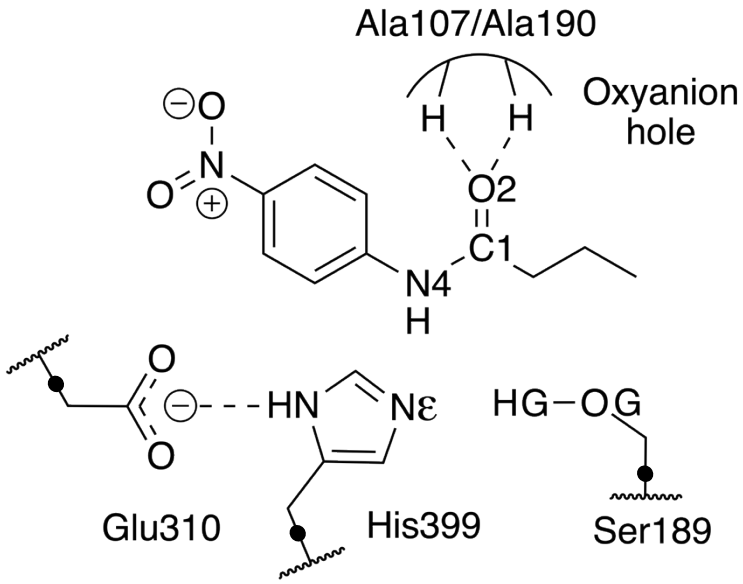

Figure S4. Schematic representation of the QM sub-set region (shadowed region). Black dots represent link atoms between QM and MM regions. The H-bond interactions between *N*-(4-nitrophenyl)-butyramide substrate and the oxyanion hole, are shown as dashed lines.

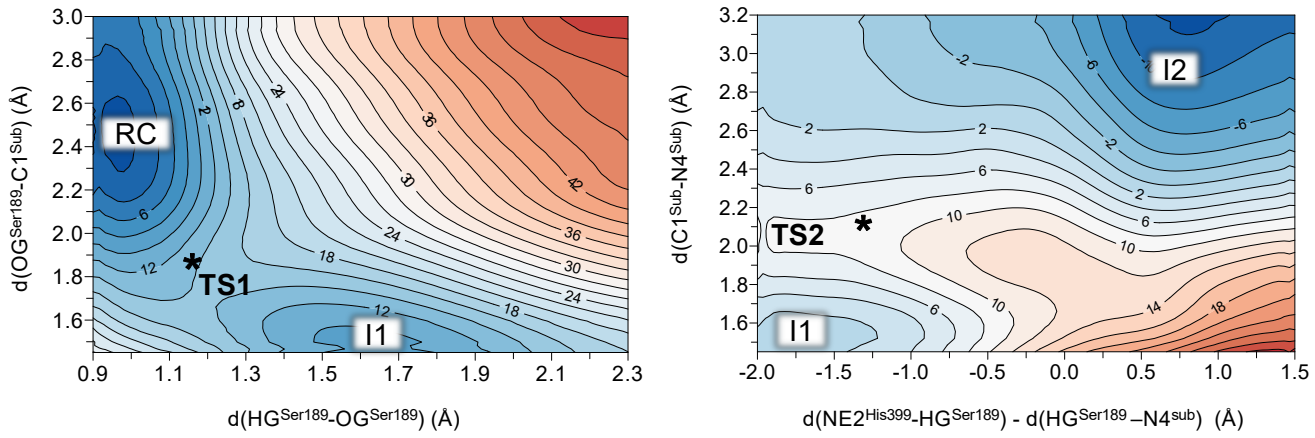

Figure S5. **M06-2X:AM1/OPLS-AA Free Energy Surfaces of F398D Bs2 variant.** Distances are given in Å and isoenergetic lines are in kcal·mol^{-1}. The black stars indicate the position of single TS structures localized at potential energy surface computed at M06-2X/OPLS-AA level of theory.

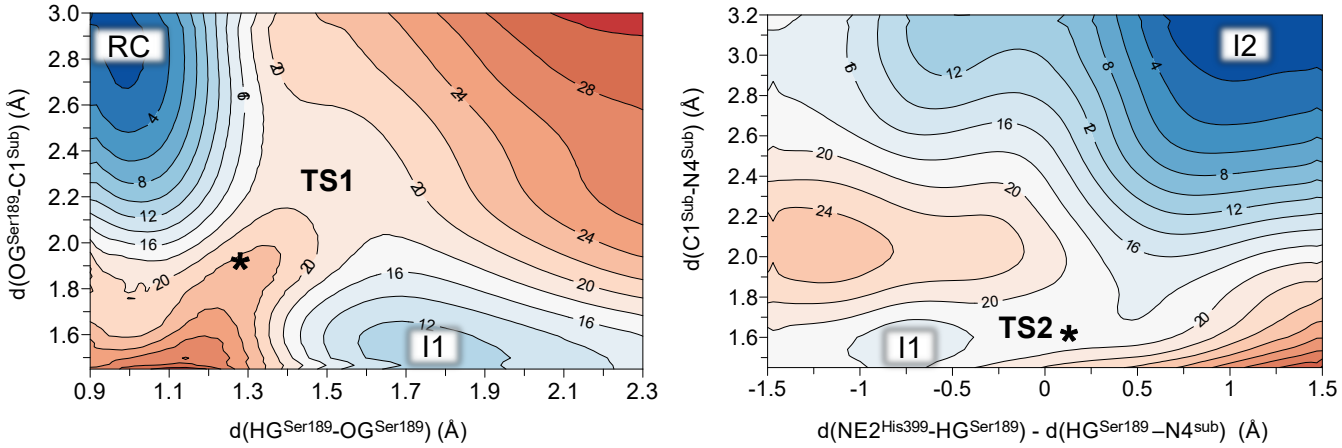

Figure S6. **M06-2X:AM1/OPLS-AA Free Energy Surfaces of F398D-H$^+$ Bs2 variant.** Distances are given in Å and isoenergetic lines are in kcal·mol^{-1}. The black stars indicate the position of single TS structures localized at potential energy surface computed at M06-2X/OPLS-AA level of theory.

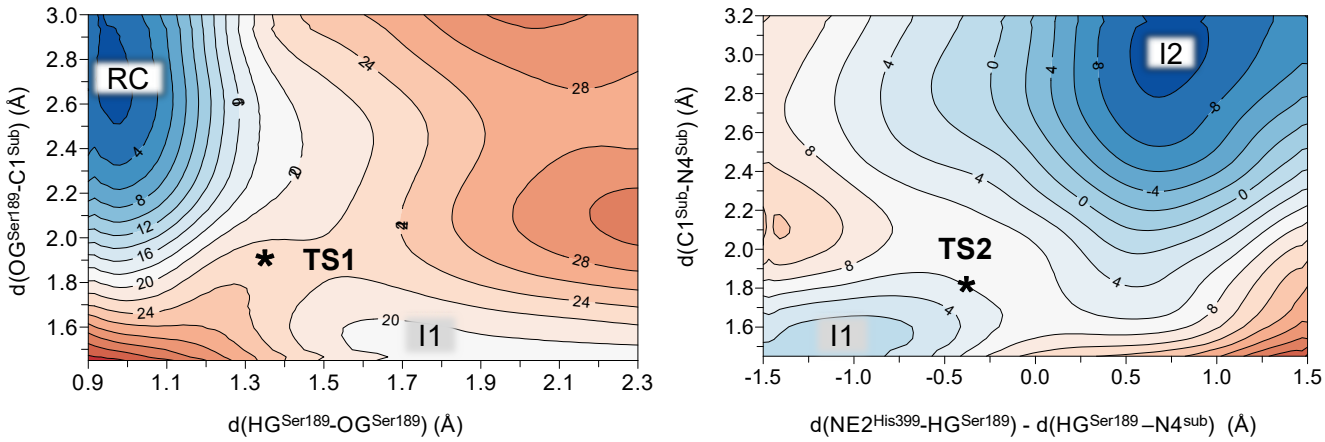

Figure S7. **M06-2X:AM1/OPLS-AA Free Energy Surfaces of D66I/L335K Bs2 variant.** Distances are given in Å and isoenergetic lines are in kcal·mol^{-1}. The black stars indicate the position of single TS structures localized at potential energy surface computed at M06-2X/OPLS-AA level of theory.

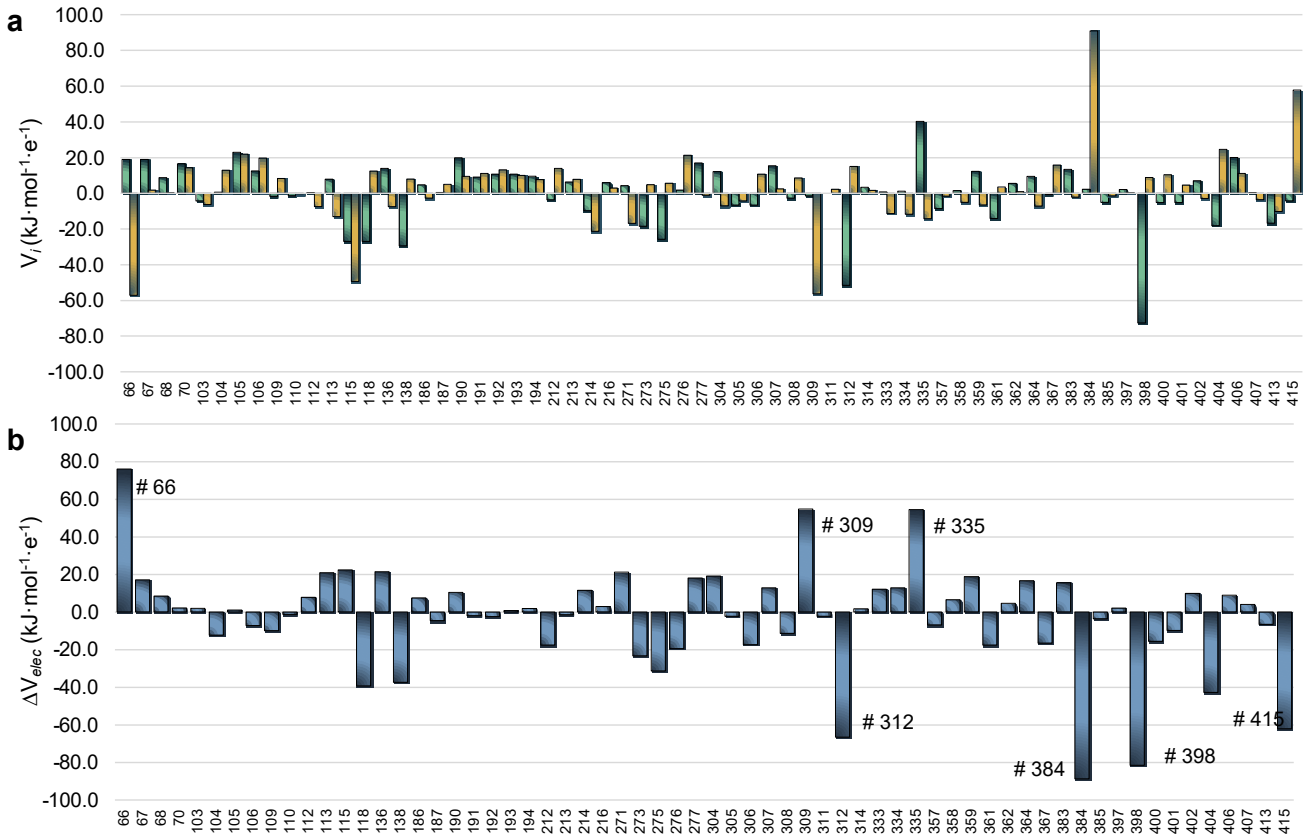

Figure S8. The electrostatic potential generated by Bs2 and CALB per residue. a, Electrostatic potential generated per residue on the Nε atom of the active site histidine (His399/His224) in the TS1 structure optimized in Bs2 (yellow bars) and in CALB (green bars). **b**, the difference in the electrostatic potential per residue between Bs2 and CALB. ΔV_{elec} values were calculated as V_i^{Bs2} - V_i^{CALB} where *i* is the corresponding residue in the aligned pairs. Only the residues within 15 Å from the center of mass of the substrate were taken into consideration.

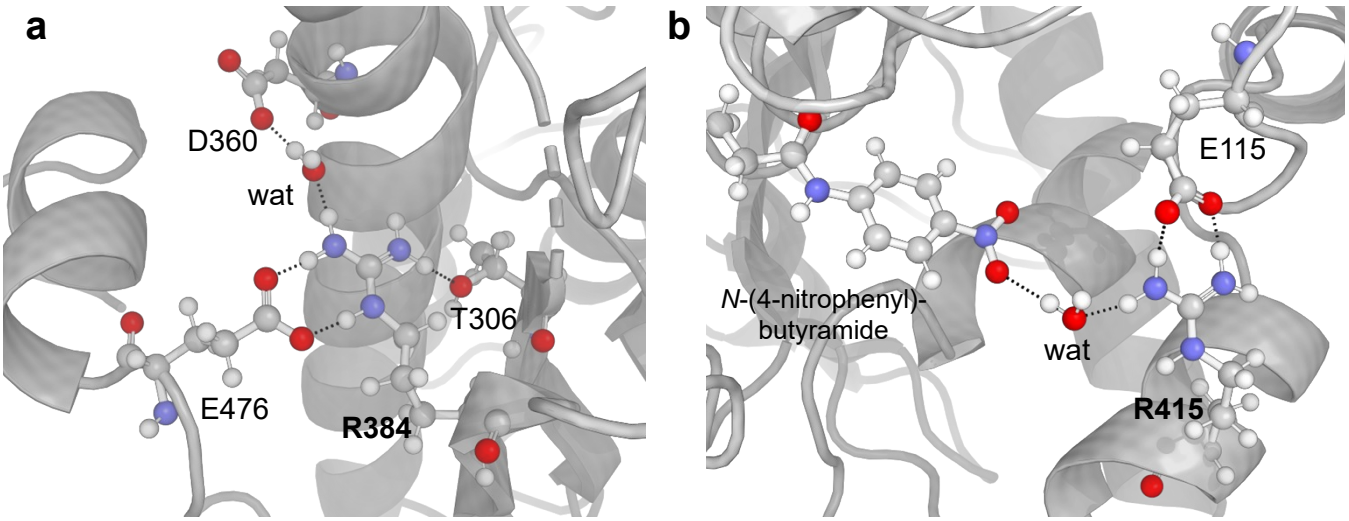

Figure S9. Detailed view of the surrounding of R384 and R415 in Bs2. a, Hydrogen bonding network of R384 with the lateral chains of E476, D360 and T306. **b,** Hydrogen bond interactions of R415 with E115 and the substrate *N*-(4-nitrophenyl)-butyramide.

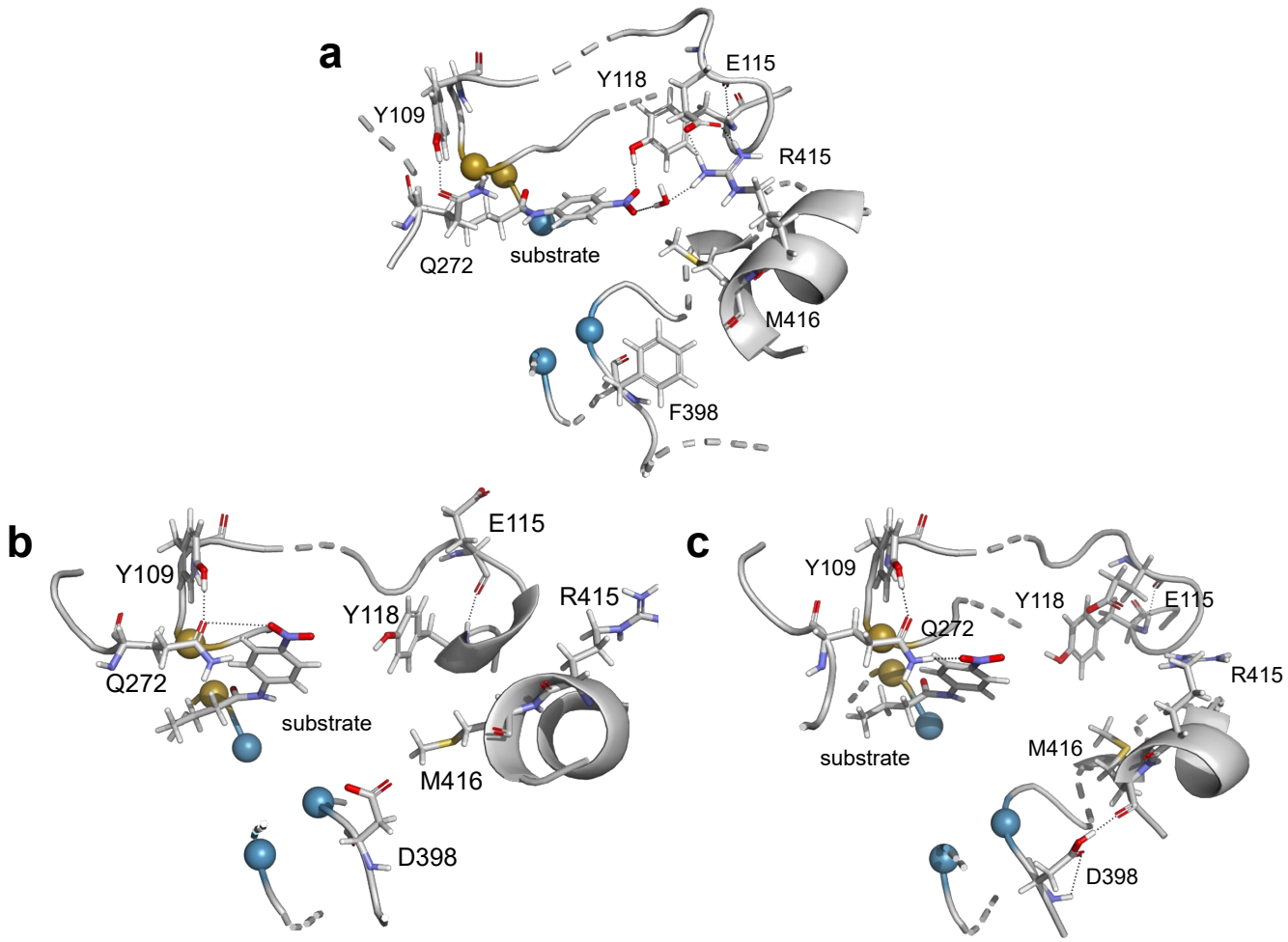

Figure S10. Detailed image of the arrangement of the substrate contacts in wild-type Bs2 and F398D-H$^+$ Bs2. a, interactions of Y118 and R415 with the nitro group of *N*-(4-nitrophenyl)-butyramide in wild-type Bs2. **b,** interactions of Y109 and Q272 with the nitro group of *N*-(4-nitrophenyl)-butyramide in F398D Bs2. **c,** interactions of Y109 and Q272 with the nitro group of *N*-(4-nitrophenyl)-butyramide in F398D-H$^+$ Bs2.The mutation F398D-H$^+$ leads to the formation of a hydrogen bond with the backbone of M416, promoting the rearrangement of the interactions with the substrate. Blue spheres represent the catalytic triad while yellow spheres are the residues involved in the oxyanion hole.

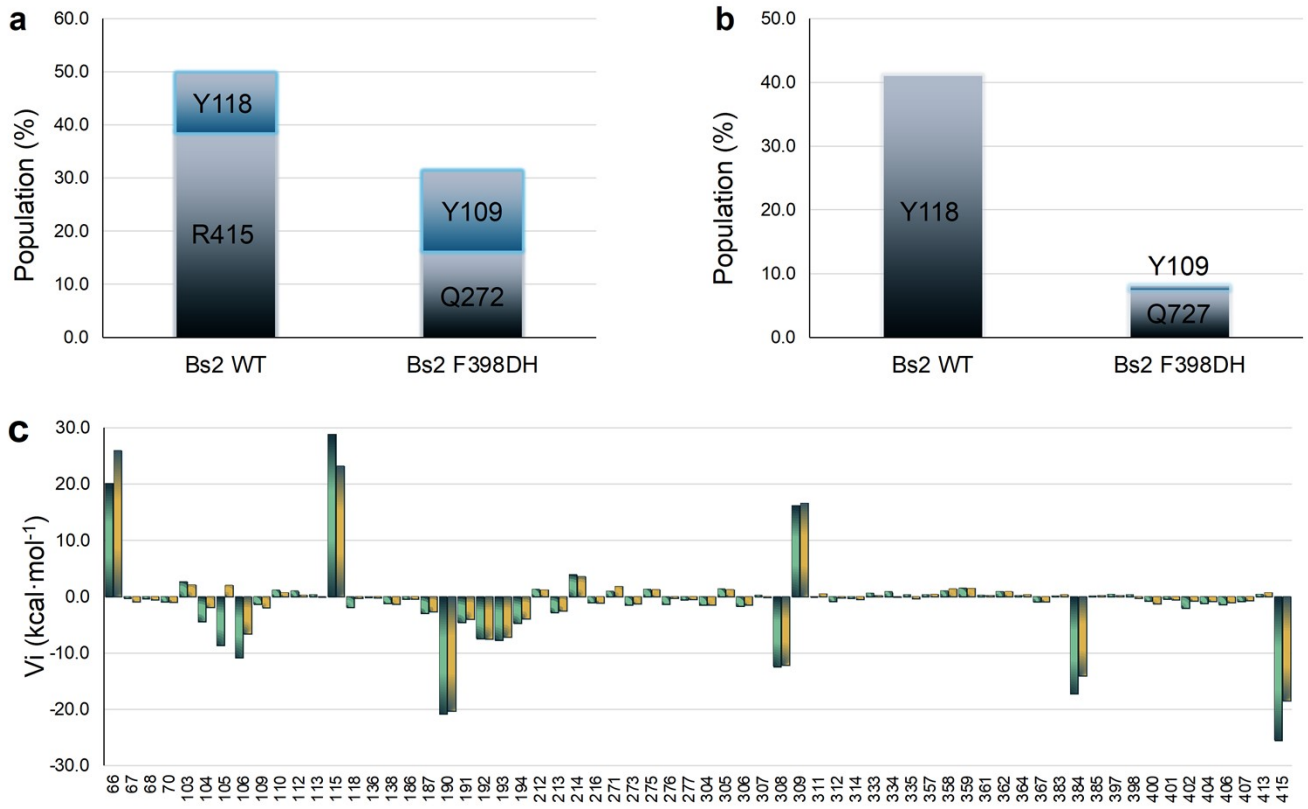

Figure S11. Analysis of contacts and interactions of wild-type Bs2 and F398D-H$^+$ Bs2 along the molecular dynamics simulation. a, water bridge contacts of key residues with the nitro group of the substrate. **b,** hydrogen bond contacts of key residues with the nitro group of the substrate. **c,** electrostatic interactions of the residues within 15 Å with the substrate along the molecular dynamics simulation. Green bars represent the interactions in the wild-type Bs2 while yellow ones correspond to the F398D-H$^+$ Bs2 variant.

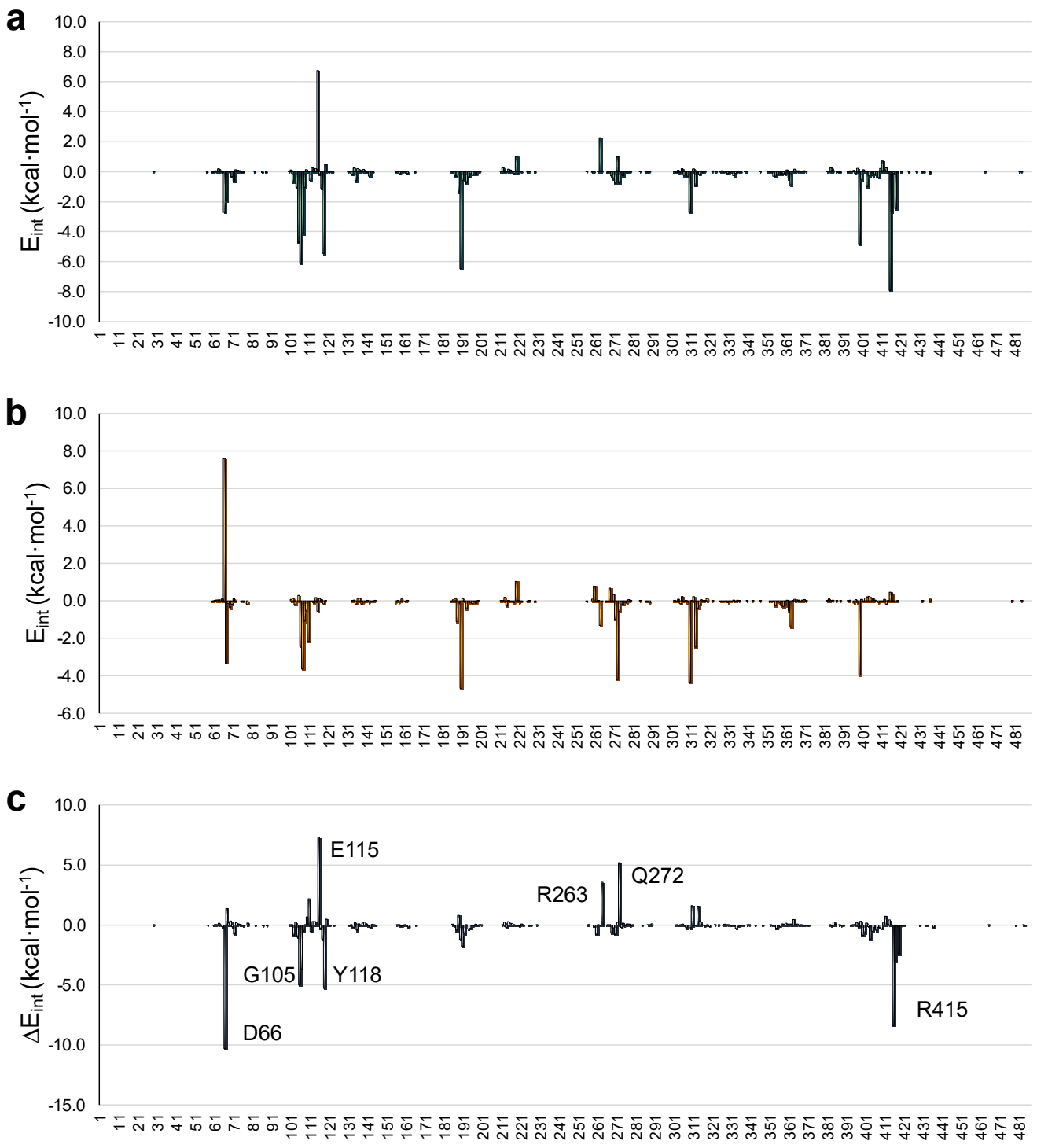

Figure S12. Interaction energies of the protein by residue with the substrate. a, interactions in wild type Bs2; **b,** interactions in the F398D-H^+ Bs2 variant; **c,** difference of interactions energies computed as $E_{int}^{wild\text{-}type} - E_{int}^{F398D\text{-}H+}$.

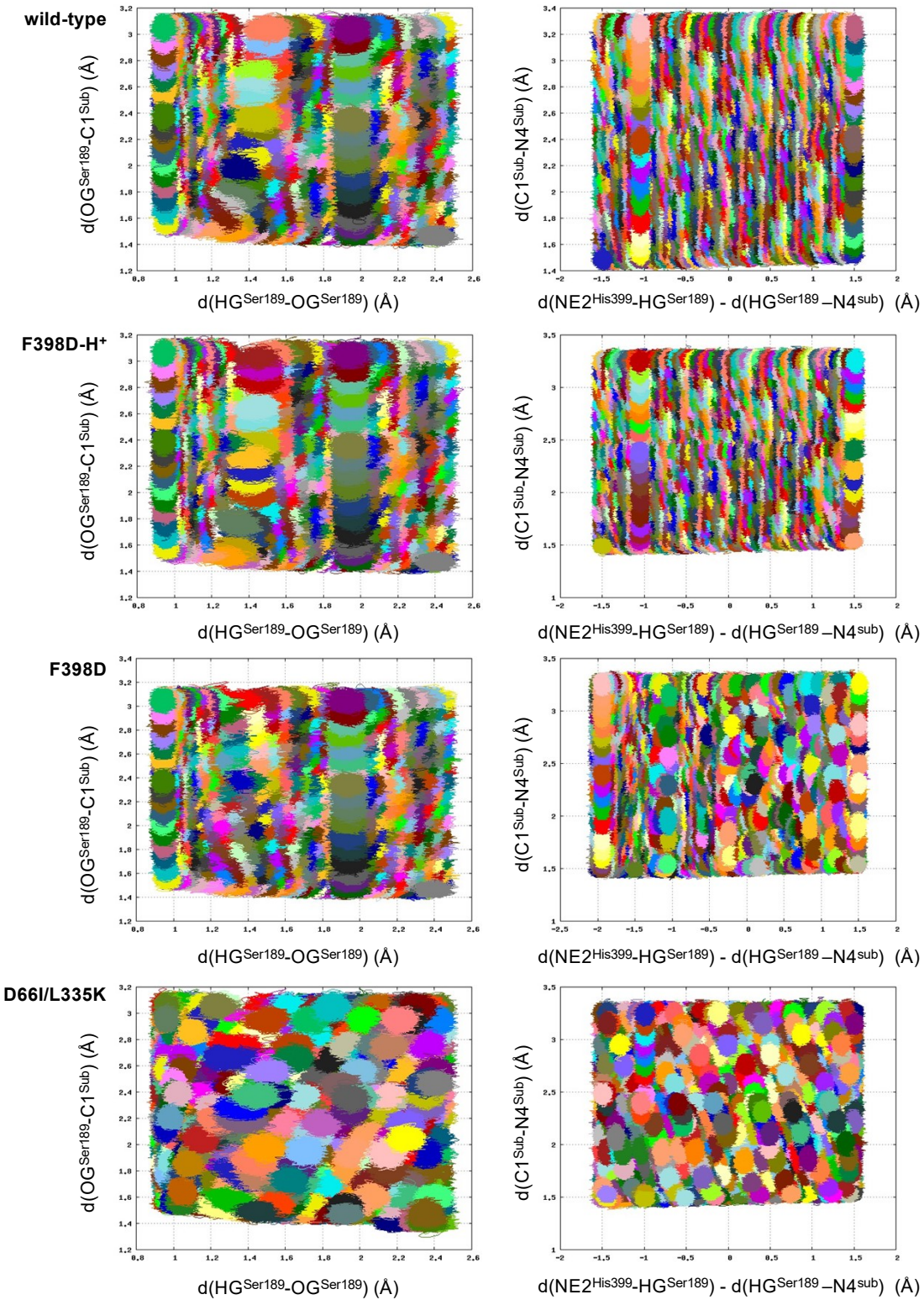

Figure S13. Representation of the overlapping between windows during the MD simulation of the Umbrella Sampling for all four Bs2 variants.

Table S1. Key inter-atomic distances of the different states appearing along the acylation step of *N*-(4-nitrophenyl)-butyramide catalyzed by F398D Bs2 variant. Structures optimized at M06-2X/MM level. All distances are given in Å.

	RC	TS1	INT1	INT1	TS2	INT2
$OG_{Ser189} - C1_{subs}$	2.26	1.87	1.50	1.48	1.38	1.32
$OG_{Ser189} - HG_{Ser189}$	1.03	1.16	1.75	1.74	1.89	2.48
$N\varepsilon_{His399} - HG_{Ser189}$	1.52	1.34	1.04	1.04	1.02	1.81
$C1_{subs} - N4_{subs}$	1.43	1.48	1.56	1.56	2.12	3.07
$HG_{Ser189} - N4_{subs}$	2.72	2.54	2.45	2.48	2.33	1.05
$HD1_{His399} - OE1_{Glu310}$	1.68	1.61	1.44	1.43	1.42	1.74
$HD1_{His399} - ND1_{His399}$	1.05	1.05	1.10	1.11	1.11	1.04
$C1_{subs} - O2_{subs}$	1.22	1.24	1.29	1.29	1.23	1.23
$O2_{subs} - H_{Ala190}$	1.80	1.83	1.71	1.71	1.66	1.75
$O2_{subs} - H_{Ala107}$	1.69	1.72	1.72	1.69	1.75	1.77

Table S2. ESP charges (in a.u.) of the key atoms of the amide substrate computed at M06-2X/MM level on the states involved in the acylation step catalyzed by the F398D Bs2 variant from reactants state (RS) to Intermediate 2 (INT2).

	RC	TS1	INT1	INT1	TS2	INT2
$C1_{subs}$	0.568	0.813	0.816	0.817	0.731	0.721
$N4_{subs}$	-0.592	-0.690	-0.628	-0.739	-0.648	-0.779
$O2_{subs}$	-0.694	-0.828	-0.983	-0.744	-0.795	-0.748
$N\varepsilon_{His399}$	-0.070	-0.057	-0.076	-0.075	-0.028	-0.352
OG_{Ser189}	-0.485	-0.479	-0.480	-0.444	-0.401	-0.399

Table S3. Key inter-atomic distances of the different states appearing along the acylation step of *N*-(4-nitrophenyl)-butyramide catalyzed by F398D-H^+ Bs2 variant. Structures optimized at M06-2X/MM level. All distances are given in Å.

	RC	TS1	INT1	INT1	TS2	INT2
$OG_{Ser189} - C1_{subs}$	2.37	1.92	1.50	1.48	1.45	
$OG_{Ser189} - HG_{Ser189}$	1.01	1.29	2.52	2.95	2.67	
$N\varepsilon_{His399} - HG_{Ser189}$	1.73	1.28	1.03	1.03	1.39	
$C1_{subs} - N4_{subs}$	1.42	1.47	1.54	1.54	1.62	
$HG_{Ser189} - N4_{subs}$	2.72	2.59	2.04	2.06	1.26	
$HD1_{His399} - OE1_{Glu310}$	1.73	1.28	1.03	1.03	1.39	
$HD1_{His399} - ND1_{His399}$	1.01	1.29	2.52	2.95	2.67	
$C1_{subs} - O2_{subs}$	1.68	1.60	1.59	1.57	1.70	
$O2_{subs} - H_{Ala190}$	1.03	1.05	1.06	1.06	1.04	
$O2_{subs} - H_{Ala107}$	1.22	1.24	1.30	1.30	1.29	

Table S4. ESP charges (in a.u.) of the key atoms of the amide substrate computed at M06-2X/MM level on the states involved in the acylation step catalyzed by the F398D-H^+ Bs2 variant from reactants state (RS) to Intermediate 2 (INT2).

	RC	TS1	INT1	INT1	TS2	INT2
$C1_{subs}$	0.755	0.959	0.930	0.853	0.745	
$N4_{subs}$	-0.776	-0.836	-0.797	-0.715	-0.395	
$O2_{subs}$	-0.692	-0.840	-0.988	-0.978	-0.950	
$N\varepsilon_{His399}$	-0.229	-0.135	-0.092	-0.092	-0.198	
OG_{Ser189}	-0.573	-0.655	-0.561	-0.540	-0.510	

Table S5. Key inter-atomic distances of the different states appearing along the acylation step of *N*-(4-nitrophenyl)-butyramide catalyzed by D66I/L335K Bs2 variant. Structures optimized at M06-2X/MM level. All distances are given in Å.

	RC	TS1	INT1	INT1	TS2	INT2
$OG_{Ser189} - C1_{subs}$	2.44	1.91	1.49	1.48	1.41	1.33
$OG_{Ser189} - HG_{Ser189}$	1.00	1.35	2.26	2.48	2.46	2.65
$N\varepsilon_{His399} - HG_{Ser189}$	1.67	1.19	1.04	1.05	1.50	1.77
$C1_{subs} - N4_{subs}$	1.35	1.41	1.53	1.55	1.82	2.70
$HG_{Ser189} - N4_{subs}$	2.68	2.62	1.89	1.76	1.12	1.04
$HD1_{His399} - OE1_{Glu310}$	1.00	1.35	2.26	2.48	2.46	2.65
$HD1_{His399} - ND1_{His399}$	1.68	1.59	1.56	1.57	1.68	1.70
$C1_{subs} - O2_{subs}$	1.04	1.05	1.06	1.06	1.04	1.03
$O2_{subs} - H_{Ala190}$	1.25	1.27	1.31	1.31	1.27	1.23
$O2_{subs} - H_{Ala107}$	2.14	1.89	1.84	1.89	1.99	1.85

Table S6. ESP charges (in a.u.) of the key atoms of the amide substrate computed at M06-2X/MM level on the states involved in the acylation step reaction catalyzed by the D66I/L335K Bs2 variant from reactants state (RS) to Intermediate 2 (INT2).

	RC	TS1	INT1	INT1	TS2	INT2
$C1_{subs}$	0.847	0.970	0.837	0.938	0.946	0.928
$N4_{subs}$	-0.858	-0.963	-0.757	-0.845	-0.680	-1.048
$O2_{subs}$	-0.905	-0.985	-1.084	-1.112	-1.059	-0.903
$N\varepsilon_{His399}$	-0.122	-0.095	-0.173	-0.211	-0.305	-0.371
OG_{Ser189}	-0.512	-0.662	-0.545	-0.615	-0.565	-0.491

Table S7. Free energies derived from the free energy surfaces computed at M06-2X for the acylation step of the four Bs2 variants. All energies are relative to RC in kcal·mol^{-1}.

	RC	TS1	I1	TS2	I2
WT	0.0	19.2	9.3	17.6	2.8
F398D	0.0	13.0	8.2	14.3	-6.8
D66I/L335K	0.0	20.8	17.7	23.5	6.1
F398D-H$^+$	0.0	18.8	10.5	12.5	-5.4

COMPUTATIONAL METHODS

Models set up. Wild type *p*-nitrobenzyl (PNB) esterase sequence from *Bacillus subtilis* (with ID P37967) that corresponds to the protein used in the experimental measurements[1] was initially taken from UniProt[2] accessible resource of protein sequence and functional information. Due to the lack of crystallized structure for this specific variant, the framework for the required model, a natural variant of the protein (strain 168), was prepared based on PNB esterase from the same organism (Bs2; PDB ID: 1QE3).[3] Both enzymes share 97.6 % of sequence identity. Thus, the X-ray structure was used as a template to build the Bs2 model by adding the missing residues and introducing required mutations. All changes were done using Modeller.[4]

Based on the structure of the wild type which was studied in the previous works[5], three variants were prepared, F398D, protonated F398D-H^+ and D66I/L335K. The protonation state of titratable residues was determined at pH 7 by estimating pKa shifts generated by the local environment on titratable groups using the empirical program PropKa ver. 3.0.3.[6,7] The values of pKa obtained for Glu188 (8.72), Glu214 (7.52), and Glu402 (10.32) ensured their protonated state. Additionally, all histidines residues present in the enzyme were found to be neutral, with pKa values varying between 4.12 and 6.19. After a detailed inspection of the surrounding of each histidine residue, it was concluded that all should be protonated in Nδ position. *N*-(4-nitrophenyl)-butyramide substrate was placed inside the active site pocket covalently bound to catalytic Ser189 in the form of intermediate 1, in order to avoid possible substrate dissociation to the solvent during MD simulations. Thus, once the hydrogen atoms were added to the structure, the counterions ions were placed in the most electrostatically favorable positions to neutralize the system. Depending on the variant of the enzyme the 21, 20 and18 sodium ions were added, for F398D, F398D-H^+ and D66I/L335K, variant of Bs2, respectively. Subsequently, the system was solvated by placing it in a $100 \times 80 \times 80$ $Å^3$ pre-equilibrated box of TIP3P[8] water molecules. Any water with an oxygen atom lying

in a radius of 2.8 Å from a heavy atom of the protein was deleted. In order to equilibrate the total system, classical MD simulations were done. For *N*-(4-nitrophenyl)-butyramide the same force field parameters were used as determined in our previous work.[9] Such prepared model was optimized, then the system was heated to 303 K with 0.1 K temperature increment and equilibrated during short (100 ps) NPT MD simulations, the proper 50 ns of non-accelerated classical MD simulations were done using the NVT ensemble with AMBER force field,[10] as implemented in NAMD software.[11] The temperature during the MD simulation was controlled using the Langevin thermostat.[12] In order to improve the time of simulations, cut-offs for nonbonding interactions were applied using a smooth switching function between 14.5 and 16 Å. During MD simulations all atoms were free to move. Periodic boundary conditions were used. Time-dependent evolution of the root mean square deviations (RMSD) for all three variants and B-factors for F398D and D66I/L335K Bs2 variants are depicted in Figure S3. All the analysis of the MD, including RMSD, B-factors and contacts was done using AmberTools.[13] Based on the RMSD obtained from MD simulations it was concluded that all three models of Bs2 variants that will be studied by QM/MM methods (F398D, F398D-H^+ and D66I/L335K) do not suffer any dramatic changes during MD simulations, and their values oscillate within the standard deviation, not higher than 0.25 Å. Thus, one structure from each of the MD simulations was chosen for further study applying QM/MM approach. The starting structures were selected by its proximity to the average values of RMSD.

QM/MM simulations. In the present work, the standard additive hybrid QM/MM scheme was used to construct the total Hamiltonian, $\hat{H}_{QM/MM}$, where the total energy $E_{QM/MM}$ is obtained as the sum of specific contributions, as presented in equation 1:

$$E_{QM/MM} = \langle \Psi \left| \hat{H}_o \right| \Psi \rangle + \left(\sum \left\langle \Psi \left| \frac{q_{MM}}{r_{e,MM}} \right| \Psi \right\rangle + \sum\sum \frac{Z_{QM} q_{MM}}{r_{QM,MM}} \right) + E_{QM/MM}^{vdW} + E_{MM} \quad (1)$$

where E_{MM} is the energy of the MM subsystem term, E_{QM-MM}^{vdW} the van der Waals interaction energy between the QM and MM subsystems and E_{QM-MM}^{elect} includes both the Coulombic interaction of the QM nuclei (Z_{QM}) and the electrostatic interaction of the polarized electronic wave function (q_{MM}) with the charges of the protein (q_{MM}). The region described by quantum mechanics includes the side chains of the catalytic Ser189, His399 and Glu310 residues as well as the full substrate, and one water molecule, as shown in Figure S4. Three-link atoms[14] were inserted where the QM/MM boundary intersected covalent bonds: these were placed between the Ca-Cb for Ser189, His299 and Glu310.

Finally, in the QM part the 55 were defined including link atoms. The rest of the protein, counterions and solvent molecules (in total 73070 atoms in F398D and F398D-H^+, and 73085 atoms in D66I/L335K variants) were represented by classical OPLS-AA force field[15] and TIP3P force fields, respectively, as implemented in fDynamo library.[16] The Austin Model 1 (AM1)[17] semiempirical Hamiltonian and the Minnesota Functional M06-2X,[18] with the standard 6-31+G(d,p) basis set, were used to treat the QM sub-set of atoms, as implemented in Mopac[19] and Gaussian 09,[20] respectively. The atom positions of all residues presented beyond 25 Å from the substrate were frozen and the same cut-offs as in MD simulations were applied for the nonbonding interactions.

Potential Energy Surfaces. Potential Energy Surfaces (PES) were explored by choosing and scanning the appropriate combination of internal coordinates (ξ_i) assuming their dominant role in the shape of the reaction coordinate. Thus, a combination of different distances was controlled during the exploration of all four chemical steps being part of the complete reaction path. In the first step of the reaction, the PES was generated by controlling the distance between nitrogen, Nε atom of His399 and hydrogen, HG atoms of Ser189, together with the distance between oxygen, OG atom of Ser189 and carbonyl carbon, C1 atom of a substrate, directing acylation process. In the second step antisymmetric combination of nitrogen, Nε

atom and hydrogen HG, attached to His399 and this hydrogen atom and its acceptor, nitrogen, N4 atom of the substrate, together with carbon-nitrogen (C1-N4) bond of a substrate were controlled.

In order to explore all PESs, the harmonic constraint of 5000 $kJ \cdot mol^{-1} \cdot Å^{-2}$ was used to maintain the proper interatomic distances along the reaction coordinate, and a series of conjugate gradient optimizations and L-BFGS-B optimization algorithms[21] were applied to obtain the final potential energy of the minimized constrained geometry. The QM sub-set of atoms was described by the Austin Model 1 (AM1) semiempirical Hamiltonian. The distances evolution was controlled by applying a small size change of 0.1 Å when the distance between two heavy atoms was explored, or 0.05 Å when the transfer of light hydrogen atom was involved.

A micro-macro iteration optimization algorithm[22,23] together with the Baker's algorithm[24,25] was used to localize, optimize, and characterize the transition states (TS) and structures using a Hessian matrix containing all the coordinates of the QM subsystem, whereas the gradient norm of the remaining movable atoms was maintained less than 0.25 kcal mol^{-1} $Å^{-1}$. the Intrinsic Reaction Coordinate[10] (IRC) were traced down from located TSs to the connecting valleys in mass-weighted Cartesian coordinates. And the same micro-macro iteration optimization algorithm was used to optimize reactant complex (RC) and intermediates (Is). The existence of the saddle-points, as well as those located in minima, was confirmed by frequency calculation. Thus, for TS structures, only one imaginary value of frequency was registered, while for structures located in the minimum of the PESs no imaginary values were found.

Free Energy Surfaces. FESs were obtained, in terms of two-dimensional potential mean force (2D-PMF),[26] for every step of the reaction using the Umbrella Sampling approach[26,27] combined with the Weighted Histogram Analysis Method (WHAM).[28] The procedure for the PMF calculation is straightforward and requires a series of molecular dynamics simulations in which the distinguished reaction coordinate variable, ξ, is constrained around particular values. The values of the variables

sampled during the simulations are then pieced together to construct a distribution function from which the PMF is obtained as a function of the distinguished reaction coordinate (W(ξ)). The PMF is related to the normalized probability of finding the system at a particular value of the chosen coordinate by eq 2:

$$W(\xi) = C - kTln\int \rho(r^N)\delta\left(\xi(r^N) - \xi\right)dr^{N-1} \tag{2}$$

The activation free energy can be then expressed as:

$$\Delta G^{\ddagger}(\xi) = W(\xi^{\ddagger}) - \left[W(\xi^R) + G_{\xi}(\xi^R)\right] \tag{3}$$

where the superscripts indicate the value of the reaction coordinate at the reactants (R), and at the TS (‡), and $G_{\xi}(\xi^R)$ is the free energy associated with setting the reaction coordinate to a specific value at the reactant state. Normally this last term makes a small contribution, and the activation free energy is directly estimated from the PMF change between the maximum of the profile and the reactant's minimum:

$$\Delta G^{\ddagger}(\xi) \approx W(\xi^{\ddagger}) - W(\xi^R) = \Delta W^{\ddagger}(\xi) \tag{4}$$

The selection of the reaction coordinate is usually trivial when the mechanism can be driven by a single internal coordinate or a simple combination (as the antisymmetric combination of two interatomic distances). However, this is not the case for all possible steps of the reaction subject of study in this paper where many coordinates are participating. Instead, we were compelled to obtain a much more computationally demanding 2D-PMF using two coordinates: ξ_1 and ξ_2. The 2D-PMF is related to the probability of finding the system at particular values of these two coordinates:

$$W(\xi) = C' - kTln\int \rho(r^N)\delta\left(\xi_1(r^N) - \xi_1\right)\delta\left(\xi_2(r^N) - \xi_2\right)dr^{N-2} \tag{5}$$

To estimate the activation free energy from this quantity, we recovered one-dimensional PMF changes tracing a maximum probability reaction path on the 2D-PMF surface and integrating over the perpendicular coordinate.

Thus, a series of MD simulations were performed adding a constraint for the selected reaction coordinates with an umbrella force constant of 2500 kJ·mol^{-1}·Å^{-2}. In every window, QM/MM MD simulations were performed with a total of 5 ps of equilibration and 20 ps of production at 303 K using the Langevin-Verlet algorithm[29] with a time step of 1 fs. Structures obtained in previously computed PESs were used as starting points for the MD simulations in every window. Finally, the WHAM was computed with a tolerance of 0.001 kcal·mol^{-1}. The overlapping between windows shown in Figure S13 is a representation of the reaction coordinates over time of every window.

Spline corrections. In order to improve lower quality results associated with the lower-level semiempirical calculations, high-level corrections were applied using Density Functional Theory (DFT). As already described in the literature,[30,31] a correction term $S[\Delta E_{LL}^{HL}(\xi_1,\xi_2)]$ is interpolated to any value along reaction coordinates in the FES. A continuous energy function is used to obtain the corrected PMFs:

$$E = E_{LL/MM} + S[\Delta E_{LL}^{HL}(\xi_1,\xi_2)] \quad (6)$$

where S is the two-dimensional spline function and ΔE_{LL}^{HL} is the difference between the energies obtained at low-level (LL) and high-level (HL) of the theory of the QM part. The AM1 semiempirical Hamiltonian was used as the LL method, while the DFT method was selected for the HL energy calculation. In particular, HL energy calculations were performed by means of the hybrid M06-2X functional using the standard 6-31+G(d,p) basis set. These calculations were carried out using the Gaussian09 program.

Structural alignment of CALB and Bs2. To compare the environment generated by the enzyme surrounding the substrate a structural alignment was done between Bs2 and CALB. For this purpose, TS1 structures localized at M06-2X/MM level in both systems were used. Due to the poor percentage of sequence identity between enzymes a structural alignment based on sequence similarity was unachievable.

For that reason, an alternative procedure was used involving the geometrical overlapping of the positions of atoms of the amide bond and the neighboring carbon atoms. Structures of protein were forced to align accordingly, which was achieved using a rotation quaternion around those selected atoms highlighted in Figure S14.

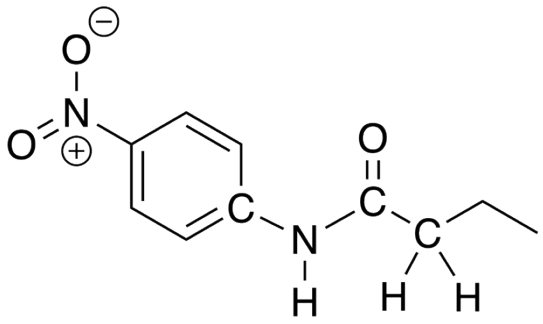

Figure S14. Structure of the substrate with highlighted atoms (in yellow) used as observed and reference points for geometrical overlapping.

The superimposition was done using quaternions implemented in QMCube.[32] This vector formulation for molecule rotations is useful in large vectorized systems. It basically assumes that the optimal superposition can be found by finding the normalized eigenvector of the smallest eigenvalue of the quaternion 4 x 4 matrix, where the components of this eigenvector represent the optimal orientation of the target structure towards the reference. Once the parameters of the quaternion are found, the molecule can be rotated applying the optimal rotation quaternion-derived matrix to the target molecule.[33]

When both proteins were aligned, structures were compared based on the position of the centers of mass of every residue inside each protein. Residues of Bs2 and CALB were paired based on the proximity of their centers of mass, i.e. the pair of a residue from Bs2 is the residue from CALB which center of mass lies the nearest to the tested residue. In order to reduce the error of alignment, the centers of mass were

averaged along a 20 ps constrained QM/MM MD on TS1 of both proteins. The pairing alignment is depicted in Figure S2.

Electrostatic potential per residue. The electrostatic potential generated on Nε of the catalytic His399 was computed. Only the residues whose center of mass lies within 15 Å of the center of mass of the substrate were considered. Electrostatic potential per residue (V_{res}) was computed based on equation 6,

$$V_{res} = \sum_{i=1}^{n} \frac{q_i}{4\pi\varepsilon \cdot r_i} \tag{6}$$

where n corresponds to the number of atoms in the residue, q_i is the charge of the atom taken from the OPLS-AA force field, and r_i is the distance between atom i and Nε of His399. Cut-offs of 14.5 and 16 Å were applied. The electrostatic potential per residue was averaged along a 20 ps constrained QM/MM MD simulation on TS1. The electrostatic potential per residue in CALB and Bs2 is depicted in Figure S3.

STRUCTURES COORDINATES

Table S8. X, Y and Z coordinates of QM atoms for Transition State Structures optimized at M06-2X/MM level for the acylation step of the F398D Bs2 variant.

Acylation step							
Transition State 1 (ν_i = -383.062 cm^{-1})				**Transition State 2** (ν_i = -166.294 cm^{-1})			
Atoms	x	y	z	Atoms	x	y	z
C	48.592	45.418	50.575	C	48.433	45.542	50.535
H	49.662	45.396	50.318	H	49.517	45.623	50.396
H	48.060	45.841	49.707	H	47.929	45.954	49.657
O	48.430	46.285	51.690	O	48.104	46.295	51.705
H	49.456	46.719	52.019	H	49.687	47.213	52.180
C	54.375	45.243	56.520	C	54.371	45.232	56.502
H	54.281	44.964	57.574	H	54.283	44.940	57.553
H	53.356	45.475	56.187	H	53.350	45.469	56.179
C	54.876	44.032	55.739	C	54.865	44.030	55.705
H	55.960	43.916	55.821	H	55.950	43.913	55.773
H	54.442	43.122	56.164	H	54.438	43.115	56.124
C	54.562	43.998	54.246	C	54.535	44.001	54.220
O	54.238	45.057	53.643	O	54.152	45.056	53.616
O	54.662	42.873	53.688	O	54.673	42.901	53.639
C	53.919	48.895	52.974	C	53.944	48.884	52.996
H	54.073	49.215	54.008	H	54.099	49.184	54.035
H	53.838	49.791	52.354	H	53.864	49.787	52.389
C	52.649	48.081	52.878	C	52.676	48.087	52.890
N	52.511	46.906	53.576	N	52.506	46.873	53.529
H	53.292	46.321	53.968	H	53.302	46.173	53.854
C	51.329	46.361	53.281	C	51.293	46.409	53.273
H	50.988	45.415	53.680	H	50.893	45.471	53.629
N	50.655	47.132	52.437	N	50.659	47.284	52.489
C	51.477	48.215	52.168	C	51.509	48.334	52.220
H	51.160	49.018	51.519	H	51.191	49.160	51.603
C	47.315	47.773	51.521	C	47.165	47.299	51.626
C	47.281	48.052	53.016	C	47.003	47.910	52.999
H	48.311	48.085	53.390	H	47.924	48.418	53.301
H	46.875	49.060	53.161	H	46.204	48.652	52.934
C	46.433	47.077	53.824	C	46.616	46.838	54.026
C	46.363	47.508	55.290	C	46.320	47.455	55.390
H	45.902	48.495	55.406	H	45.464	48.135	55.353
H	45.775	46.805	55.886	H	46.092	46.683	56.130
H	47.365	47.560	55.730	H	47.179	48.024	55.757
H	45.426	47.022	53.395	H	45.745	46.275	53.668
H	46.864	46.075	53.734	H	47.437	46.118	54.110
O	46.322	47.400	50.873	O	46.259	47.255	50.790
N	48.296	48.615	50.794	N	48.552	48.624	50.721
H	48.815	48.115	50.082	H	49.171	48.183	50.038
C	48.279	49.969	50.657	C	48.486	49.927	50.517
C	49.254	50.573	49.814	C	49.334	50.623	49.581
C	49.393	51.940	49.752	C	49.410	51.987	49.577
C	48.546	52.757	50.514	C	48.595	52.751	50.445
C	47.505	52.203	51.263	C	47.624	52.109	51.245
C	47.356	50.830	51.310	C	47.558	50.743	51.263
H	46.521	50.419	51.861	H	46.816	50.249	51.877
H	46.827	52.851	51.813	H	46.952	52.708	51.852
N	48.800	54.168	50.593	N	48.838	54.121	50.608
O	49.705	54.646	49.898	O	49.736	54.662	49.925
O	48.127	54.843	51.358	O	48.185	54.760	51.439
H	50.170	52.382	49.140	H	50.101	52.495	48.916
H	49.926	49.945	49.236	H	49.969	50.042	48.915
H	54.745	48.390	52.724	H	54.763	48.375	52.732
H	54.945	46.063	56.473	H	54.943	46.051	56.460
H	48.295	44.474	50.721	H	48.201	44.582	50.688

Table S9. X, Y and Z coordinates of QM atoms for Transition State Structures optimized at M06-2X/MM level for the acylation step of the F398D-H^+ Bs2 variant.

Acylation step							
Transition State 1 (ν_i = -1051.441 cm^{-1})				**Transition State 2** (ν_i = -1007.015 cm^{-1})			
Atoms	x	y	z	Atoms	x	y	z
C	44.224	43.709	52.695	C	44.120	43.553	52.600
H	45.016	44.388	53.034	H	44.818	44.208	53.136
H	43.741	44.205	51.837	H	43.702	44.112	51.754
O	43.277	43.587	53.748	O	43.094	43.153	53.494
H	43.563	44.229	54.828	H	42.608	45.205	55.131
C	46.591	41.656	59.922	C	46.585	41.711	59.882
H	46.396	40.633	60.262	H	46.441	40.677	60.215
H	45.929	41.798	59.060	H	45.906	41.841	59.032
C	48.059	41.728	59.453	C	48.037	41.859	59.389
H	48.748	41.867	60.293	H	48.727	42.068	60.213
H	48.318	40.769	58.993	H	48.354	40.906	58.954
C	48.442	42.787	58.415	C	48.341	42.899	58.303
O	47.692	43.766	58.202	O	47.502	43.785	58.014
O	49.528	42.592	57.771	O	49.460	42.761	57.701
C	44.854	46.163	59.331	C	44.963	46.184	59.563
H	44.434	45.531	60.117	H	44.626	45.458	60.307
H	44.290	47.099	59.343	H	44.419	47.111	59.762
C	44.606	45.457	57.988	C	44.516	45.693	58.195
N	45.247	44.271	57.714	N	44.977	44.533	57.615
H	46.099	43.911	58.201	H	45.818	44.014	57.927
C	44.870	43.824	56.519	C	44.316	44.326	56.468
H	45.242	42.917	56.068	H	44.483	43.488	55.806
N	43.978	44.634	55.967	N	43.425	45.285	56.257
C	43.806	45.678	56.879	C	43.558	46.161	57.325
H	43.150	46.508	56.666	H	42.972	47.066	57.399
C	41.489	44.046	53.220	C	41.788	43.751	53.327
C	40.814	43.087	54.194	C	40.915	42.908	54.281
H	41.436	42.997	55.089	H	41.515	42.644	55.158
H	39.869	43.531	54.527	H	40.060	43.482	54.648
C	40.543	41.728	53.554	C	40.413	41.647	53.579
C	39.713	40.809	54.446	C	39.484	40.810	54.455
H	40.217	40.615	55.398	H	39.988	40.493	55.374
H	38.736	41.254	54.669	H	38.593	41.379	54.743
H	39.538	39.845	53.960	H	39.151	39.909	53.932
H	40.023	41.886	52.602	H	39.894	41.947	52.662
H	41.498	41.258	53.294	H	41.271	41.048	53.255
O	41.418	43.853	51.993	O	41.390	43.874	52.105
N	41.587	45.436	53.676	N	42.021	45.203	54.016
H	42.500	45.899	53.528	H	42.773	45.693	53.489
C	40.541	46.277	53.893	C	40.916	46.117	54.079
C	40.840	47.631	54.214	C	41.188	47.419	54.527
C	39.857	48.508	54.599	C	40.159	48.306	54.800
C	38.528	48.062	54.679	C	38.847	47.873	54.614
C	38.182	46.772	54.272	C	38.550	46.630	54.067
C	39.170	45.902	53.843	C	39.593	45.760	53.775
H	38.878	44.927	53.474	H	39.379	44.807	53.311
H	37.141	46.463	54.285	H	37.519	46.344	53.890
N	37.546	48.930	55.255	N	37.756	48.713	55.090
O	36.488	48.457	55.666	O	36.640	48.222	55.173
O	37.800	50.126	55.349	O	38.006	49.863	55.420
H	40.102	49.525	54.881	H	40.362	49.298	55.185
H	41.878	47.947	54.184	H	42.225	47.713	54.674
H	45.807	46.345	59.577	H	45.936	46.344	59.731
H	46.321	42.276	60.659	H	46.306	42.313	60.631
H	44.673	42.872	52.383	H	44.625	42.750	52.283

Table S10. X, Y and Z coordinates of QM atoms for Transition State Structures optimized at M06-2X/MM level for the acylation step of the reaction of the D66I/L335K Bs2 variant.

Acylation step							
Transition State 1 (ν_i = -672.467 cm^{-1})				**Transition State 2** (ν_i = -164.117 cm^{-1})			
Atoms	x	y	z	Atoms	x	y	z
C	49.182	44.719	50.456	C	48.981	44.552	50.594
H	50.226	44.892	50.135	H	50.054	44.765	50.484
H	48.556	45.251	49.722	H	48.465	45.130	49.825
O	48.999	45.298	51.728	O	48.584	44.996	51.886
H	50.048	45.931	52.289	H	49.691	47.074	52.602
C	56.620	42.266	55.271	C	56.638	42.244	55.295
H	57.285	41.778	54.562	H	57.297	41.782	54.563
H	56.600	41.615	56.154	H	56.604	41.553	56.145
C	55.225	42.300	54.624	C	55.240	42.304	54.642
H	54.794	41.296	54.679	H	54.810	41.297	54.674
H	54.528	42.972	55.132	H	54.545	42.966	55.164
C	55.293	42.651	53.140	C	55.262	42.681	53.161
O	54.604	43.623	52.716	O	54.605	43.684	52.783
O	55.996	41.942	52.379	O	55.892	41.934	52.354
C	54.411	47.214	54.198	C	54.512	47.275	54.324
H	54.512	46.974	55.260	H	54.611	46.983	55.372
H	54.380	48.303	54.117	H	54.554	48.366	54.281
C	53.089	46.644	53.702	C	53.167	46.834	53.809
N	52.913	45.278	53.650	N	52.856	45.515	53.571
H	53.678	44.558	53.609	H	53.531	44.727	53.543
C	51.718	45.010	53.127	C	51.613	45.460	53.061
H	51.330	44.018	52.946	H	51.115	44.541	52.785
N	51.074	46.134	52.856	N	51.091	46.668	52.970
C	51.914	47.179	53.216	C	52.052	47.539	53.434
H	51.617	48.212	53.117	H	51.883	48.605	53.468
C	47.515	46.489	51.918	C	47.638	46.020	52.072
C	46.965	45.800	53.156	C	47.055	45.819	53.461
H	45.996	46.286	53.351	H	46.428	46.693	53.680
H	46.748	44.770	52.858	H	46.378	44.963	53.333
C	47.795	45.816	54.434	C	48.022	45.535	54.601
C	47.070	45.048	55.537	C	47.256	45.026	55.818
H	46.894	44.009	55.238	H	46.720	44.103	55.571
H	47.634	45.048	56.471	H	47.915	44.824	56.664
H	46.091	45.496	55.743	H	46.511	45.760	56.144
H	48.770	45.363	54.233	H	48.745	44.784	54.267
H	47.985	46.839	54.782	H	48.594	46.434	54.859
O	46.869	46.370	50.835	O	46.810	46.281	51.143
N	48.131	47.722	52.211	N	48.676	47.490	52.366
H	48.244	47.977	53.188	H	48.376	47.936	53.240
C	48.510	48.685	51.283	C	48.815	48.485	51.367
C	48.365	50.045	51.611	C	48.327	49.783	51.575
C	48.767	51.032	50.724	C	48.601	50.797	50.665
C	49.334	50.656	49.511	C	49.351	50.490	49.534
C	49.509	49.315	49.167	C	49.827	49.204	49.285
C	49.084	48.331	50.046	C	49.549	48.201	50.204
H	49.240	47.283	49.820	H	49.967	47.208	50.069
H	50.028	49.068	48.246	H	50.463	49.027	48.423
N	49.793	51.678	48.584	N	49.721	51.557	48.606
O	49.847	52.845	48.981	O	49.603	52.720	48.989
O	50.099	51.346	47.455	O	50.129	51.248	47.504
H	48.648	52.081	50.971	H	48.275	51.815	50.846
H	47.939	50.332	52.568	H	47.795	50.023	52.491
H	55.217	46.873	53.715	H	55.287	46.905	53.812
H	57.020	43.146	55.525	H	57.052	43.101	55.601
H	49.012	43.738	50.360	H	48.846	43.571	50.455

EXPERIMENTAL METHODS

General information. Deionized water was obtained by an *Elga PURELAB Option* system (15 MΩ·cm). Analytical Thin Layer Chromatography (TLC) was carried out with silica gel 60 F254 aluminum sheets from *Merck*. Detection was carried out using UV light (λ = 254 nm and 366 nm), followed by immersion in permanganate or cerium ammonium molybdate staining solution with subsequent development via careful heating with a heat gun. Flash column chromatography was performed using silica gel (pore size 60 Å, 0.040-0.063 mm). *N*-(4-nitrophenyl)-butyramide was synthesized using a known procedure.[9] All other solvents and reagents were obtained from commercial sources and used as received.

Plasmid miniprep-kit and gel extraction-kit were purchased from *Qiagen*. DNA oligos were purchased from *Sigma-Aldrich*. The gene encoding for wild-type Bs2[1] with a C-terminal His-tag (see below) was purchased as a double-stranded fragment form *Thermo Fisher Scientific GeneArt*. Gibson Assembly was performed using *New England Biolabs NEBuilder® HiFi DNA Assembly* master mix. Restriction enzymes and required reagents were obtained from *Thermo Fisher Scientific*. *Takara PrimeSTAR Max* was employed for site-directed mutagenesis. All kits and enzymes were used exactly following the manufacturers' protocols. DNA sequencing of constructed plasmids and mutants was obtained from *Eurofins Genomics* using T7 promoter and terminator primers.

A *VWR 3510* benchtop pH Meter connected to a *Jenway* micro pH electrode or a *VWR Universal* pH electrode were used for the pH adjustment of buffers and reaction mixtures employing either 1.0 M or 0.1 M sodium hydroxide solution or hydrochloric acid.

Size exclusion chromatography was performed using a *GE Healthcare ÄKTA Purifier* workstation or a *Bio-Rad NGC Medium-Pressure Liquid Chromatography System*.

Protein concentrations were determined using a *Thermo Scientific NanoDrop One* spectrophotometer measuring the absorption at 280 nm using the extinction coefficients obtained from https://web.expasy.org/protparam/.

Protein liquid chromatography-mass spectrometry (LC-MS) was performed on a *Waters Acquity H-Class UPLC* system combined with a *Waters Synapt G2-Si* quadrupole time of flight mass spectrometer. A *Waters Acquity UPLC Protein C4 BEH* column 300 Å, 1.7 µm (2.1 × 100 mm) held at 60 °C was applied. A flow rate of 0.2 mL/min and the gradient of eluents A and B highlighted below were employed.

Time / min	**A (H_2O, 0.1% CHO_2H) / %**	**B (ACN, 0.1% CHO_2H) / %**
0	95	5
3	95	5
50	35	65
52	3	97
54	3	97
56	95	5
60	95	5

The data was collected in positive electrospray ionization mode and analyzed using *Waters MassLynx 4.1*. Deconvoluted mass spectra were generate using the maximum entropy 1 (*MaxEnt 1*) software.

Cloning, expression and purification of recombinant proteins. The gene encoding for the wild-type Bs2 with a C-terminal linker and His-tag (`GSSHHHHHHSSG`), and 27 and 20 bases either side complimentary to the vector was purchased as a double-stranded fragment. After a NcoI and BamHI restriction enzyme digested pET28a vector the wild-type Bs2 gene was cloned in-between by Gibson assembly. The incorporation of the wild-type Bs2 gene was confirmed by DNA sequencing. Finally, Bs2 F398D was prepared by site-directed mutagenesis.

The plasmid containing the gene for Bs2 F398D was transformed into Ca^{2+} chemically competent BL21 (DE3) cells and grown on LB agar plates supplemented with kanamycin (50 µg/mL) at 37 °C overnight. One colony from the plate was picked to inoculate a 10 mL LB starter culture containing kanamycin (50 µg/mL) and grown at 37 °C and 180 rpm overnight. The starter culture was diluted into 1 L of fresh LB media containing kanamycin (50 µg/mL). The cells were grown at 37 °C and 200 rpm, until they reached an OD600 of 0.8, and IPTG was added to reach a final concentration of 1.0 mM. The cells were then incubated overnight at 20 °C. The cultures were harvested by centrifugation (4,000 rpm, 4 °C, 30 min) and the dry pellet was stored at –20 °C.

The pellet was subjected to a freeze-thaw cycle, resuspended in 25 mL of lysis buffer 1 (50 mM NaP_i, 300 mM NaCl, pH 7.5) and lysed by sonication (7 min, 5 s on, 10 s off). The insoluble fraction was removed by centrifugation at 18000 rpm for 25 min at 4 °C. The supernatant was mixed with 3 mL of Ni-NTA affinity resin for His-tag affinity purification which was equilibrated with the lysis buffer. After incubation at 4 °C for 0.5 h the resin was washed twice with 1.5 volumes of resin wash buffer 1 (50 mM NaP_i, 300 mM NaCl, 10 mM imidazole, pH 7.5). The protein was eluted with elution buffer (5× resin volume, 50 mM NaP_i, 300 mM NaCl, 250 mM imidazole, pH 7.5). Samples of the wash and elution fractions were collected and run on SDS-PAGE gel (12% w/v). The elution fractions containing the respective Bs2 variant were pooled and concentrated to 5 mL using *Amicon* ultra centrifugation with a 10 kDa cutoff. The concentrated protein solution was applied to size exclusion chromatography (*Generon ProSEC 26/60 3-70 HR* column, 50 mM NaP_i, pH 7.0). Fractions containing protein (analysis by following 280 nm UV trace) were collected and the samples loaded on SDS-PAGE to check the purity of the protein (12% w/v). Fractions containing the respective Bs2 variant were pooled, transferred to a centrifugal concentrator with a 10 kDa cutoff, and were concentrated to 15–20 mg/mL as determined by nanodrop measurement at 280 nm, with ε_{280} = 80330 M^{-1} cm^{-1} calculated using https://web.expasy.org/protparam.

The protein solutions were stored at 4 °C until further usage within a week. It should be noted that the solutions showed no significant loss in activity over 4 weeks (longer stability has not been monitored) and only minimal protein precipitation was observed.

Site-directed mutagenesis. The F398D mutation was introduced by site-directed mutagenesis PCR using *Takara PrimeSTAR Max* polymerase and the accompanying buffers, dNTPs and primers mentioned below. A 50 µL PCR reaction was prepared according to the instructions, the reaction mixture was distributed equally (12.5 µL) over 4 PCR tubes, and four different annealing temperatures in 2 °C increments were used. The PCR products were analyzed by agarose gel, correct size bands extracted, and clones of each plasmid sent for DNA sequencing. Primers used are given in the following with the site of mutation marked in bold red.

Forward primer: ACCTCCGTATAACAAAGCA**GAT**CATGCACTGG

Reverse primer: CTTTGTTATACGGAGGTTTTTTCGGATGCC

Nucleotide sequence.

ATGACCCACCAGATTGTTACCACACAGTATGGTAAAGTGAAAGGCACCACCGAAAATGGTGTTCATAAA
TGGAAAGGTATCCCGTATGCAAAACCGCCTGTTGGTCAGTGGCGTTTTAAAGCACCGGAACCGCCTGAA
GTTTGGGAAGATGTTCTGGATGCAACCGCATATGGTAGCATTTGTCCGCAGCCGAGCGATCTGCTGAGC
CTGAGCTATACCGAACTGCCTCGTCAGAGCGAAGATTGTCTGTATGTTAATGTTTTTGCACCGGATACG
CCGAGCAAAAATCTGCCGGTTATGGTTTGGATTCATGGTGGTGCATTTTATCTTGGTGCAGGTAGCGAA
CCGCTGTATGATGGTAGCAAACTGGCAGCACAGGGTGAAGTTATTGTTGTTACCCTGAATTATCGTCTG
GGTCCGTTTGGTTTTCTGCATCTGAGCAGCTTTAATGAAGCCTATAGCGATAATCTGGGTCTGCTGGAT
CAGGCAGCAGCACTGAAATGGGTTCGTGAAAACATTAGCGCATTTGGTGGTGATCCGGATAATGTTACC
GTTTTTGGTGAAAGTGCCGGTGGTATGAGCATTGCAGCACTGCTGGCCATGCCTGCAGCAAAAGGTCTG
TTTCAGAAAGCAATTATGGAAAGCGGTGCAAGCCGTACCATGACCAAAGAACAGGCAGCAAGTACCAGC
GCAGCATTTCTGCAGGTTCTGGGTATTAATGAAGGTCAGCTGGATAAACTGCATACCGTTAGCGCAGAA
GATTTACTGAAAGCAGCAGATCAGCTGCGTATTGCAGAAAAAGAAAACATCTTTCAGCTGTTTTTTCAG
CCTGCACTGGATCCGAAAACACTGCCGGAAGAACCGGAAAAAGCAATTGCAGAAGGTGCAGCAAGCGGT
ATTCCGCTGCTGATTGGTACAACCCGTGATGAAGGTTACCTGTTTTTTACTCCGGATAGTGATGTTCAT
AGCCAAGAAACCCTGGATGCAGCCCTGGAATATCTGCTGGGTAAACCGCTGGCCGAAAAAGTTGCAGAT
CTGTATCCGCGTAGCCTGGAAAGCCAGATTCATATGATGACGGATCTGCTGTTTTGGCGTCCGGCAGTT
GCATATGCCAGCGCACAGAGCCATTATGCACCGGTTTGGATGTATCGTTTTGATTGGCATCCGAAAAAA

CCTCCGTATAACAAAGCA**TTT**CATGCACTGGAACTGCCGTTTGTTTTTGGTAATCTGGATGGTCTGGAA
CGTATGGCAAAAGCAGAAATTACCGATGAAGTGAAACAACTGAGCCATACCATTCAGAGCGCATGGATT
ACCTTTGCAAAAACCGGTAATCCGAGCACCGAAGCAGTTAATTGGCCTGCATATCATGAAGAAACCCGT
GAAACCCTGATTCTGGATAGCGAAATTACCATTGAAAATGATCCGGAAAGCGAGAAACGTCAGAAACTG
TTTCCGAGCAAAGGTGAAGGTAGCAGCCATCACCATCATCATCATAGCAGTGGTTAA

Protein sequence.

MTHQIVTTQYGKVKGTTENGVHKWKGIPYAKPPVGQWRFKAPEPPEVWEDVLDATAYGSICPQPSDLLS
LSYTELPRQSEDCLYVNVFAPDTPSKNLPVMVWIHGGAFYLGAGSEPLYDGSKLAAQGEVIVVTLNYRL
GPFGFLHLSSFNEAYSDNLGLLDQAAALKWVRENISAFGGDPDNVTVFGESAGGMSIAALLAMPAAKGL
FQKAIMESGASRTMTKEQAASTSAAFLQVLGINEGQLDKLHTVSAEDLLKAADQLRIAEKENIFQLFFQ
PALDPKTLPEEPEKAIAEGAASGIPLLIGTTRDEGYLFFTPDSDVHSQETLDAALEYLLGKPLAEKVAD
LYPRSLESQIHMMTDLLFWRPAVAYASAQSHYAPVWMYRFDWHPKKPPYNKA**F**HALELPFVFGNLDGLE
RMAKAEITDEVKQLSHTIQSAWITFAKTGNPSTEAVNWPAYHEETRETLILDSEITIENDPESEKRQKL
FPSKGEGSSHHHHHHSSG*

Protein Mass. wild-type Bs2 (−Met) = 55140.21 Da
Bs2 F398D (−Met) = 55108.12 Da

96 well-plate kinetic assay. Stock solutions of the Bs2 variant (in 50 mM NaP_i, pH 7.0) and *N*-(4-nitrophenyl)-butyramide (in DMSO) were prepared. The protein stock solution was kept on ice until use and was freshly prepared before each usage. DMSO and and substrate stock solution were added to wells of a 96 transparent well-plate to a total of 15 µL. Buffer (50 mM NaP_i, pH 7.0) was added to a total volume of 135 µL (150 µL in case of controls to monitor substrate stability). The plate was transferred into a platereader, double orbitally shaken for 5 s and the absorption at λ_{Ex} = 405 nm measured to check correct substrate distribution. This data point is included in the kinetic profiles as start point, but not included in the linear fits. Then 15 µL of protein stock solution were added to each well except the enzyme free controls within 5 min. Final assay conditions were 150 µL volume, 10% DMSO, *N*-(4-nitrophenyl)-butyramide (10, 50, 100, 250 500, 1000, 2000, 3000 µM), 20 µg/mL protein. The plate was sealed with an airtight and UV-Vis transparent self-adhesive plastic cover sheet. After sealing, the plate was placed into the plate reader and the assay was monitored using the following program:

Temperature: 21.0 ± 1.0 °C

Number of repeats:	42
Delay between repeats:	1200 s
Shaking duration:	5.0 s
Shaking diameter:	0.70 mm
Shaking type:	Double orbit
Delay duration:	5.0 s
Wavelength λ_{Ex}:	405 nm

Kinetic assay analysis. In order to convert the absorption reading obtained from the kinetic assay into concentrations for the determination of kinetic data a calibration curve was generated using 10, 50, 100, 250 500, 1000, 2000, 3000 µM of 4-nitroaniline in 150 µL buffer (50 mM NaP_i, pH 7.0, 10% DMSO). Raw absorption data was converted into product concentrations and data analysis with *Origin 2020* was performed to obtained kinetic data assuming Michaelis–Menten kinetics. The maximum velocities v_{max} were obtained from the linear range of the product concentration vs. time plots and used to calculate k_{cat} and K_M for Bs2 F398D applying the enzyme kinetics / Michaelis–Menten kinetics fitting functions implemented in the software.

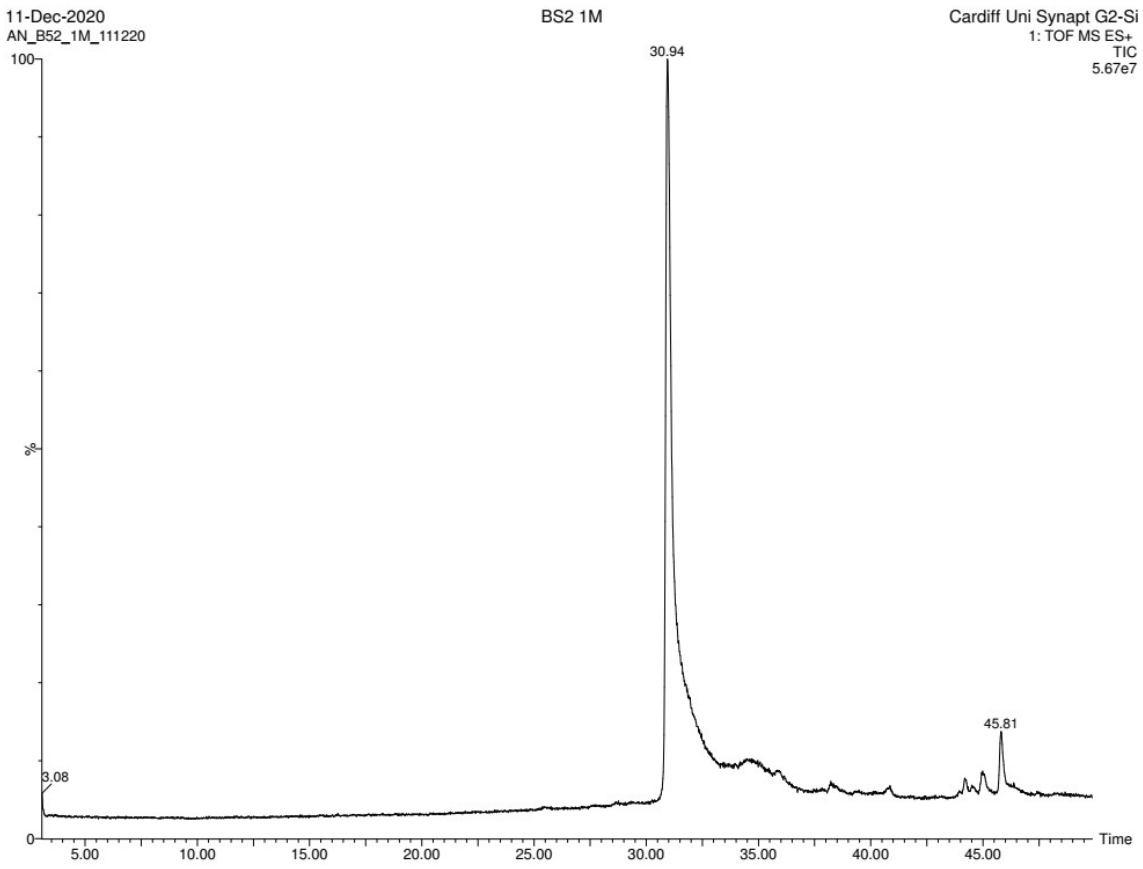

Figure S15. LC chromatogram of purified Bs2 F398D.

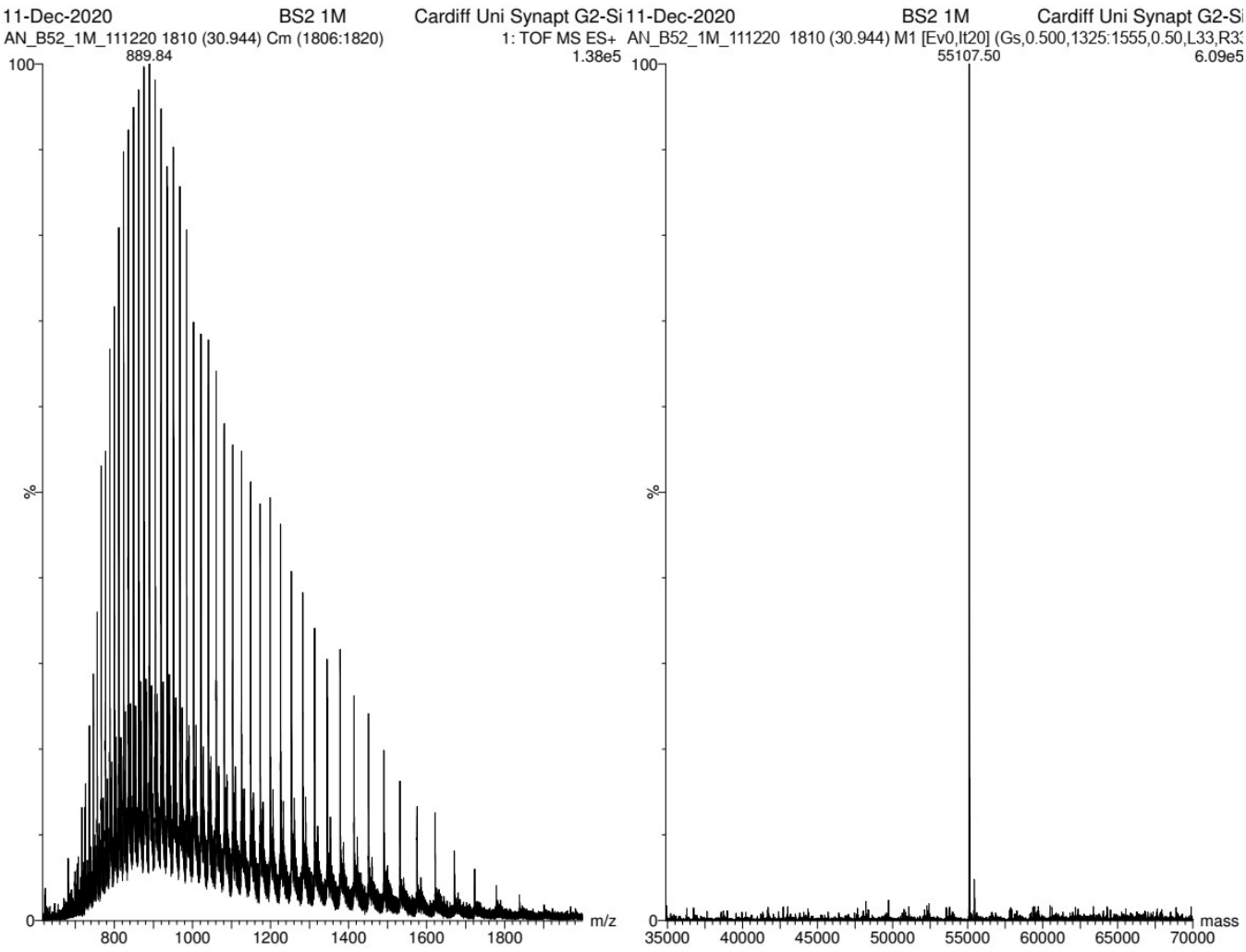

Figure S16. Raw and deconvoluted mass spectrum of purified Bs2 F398D.

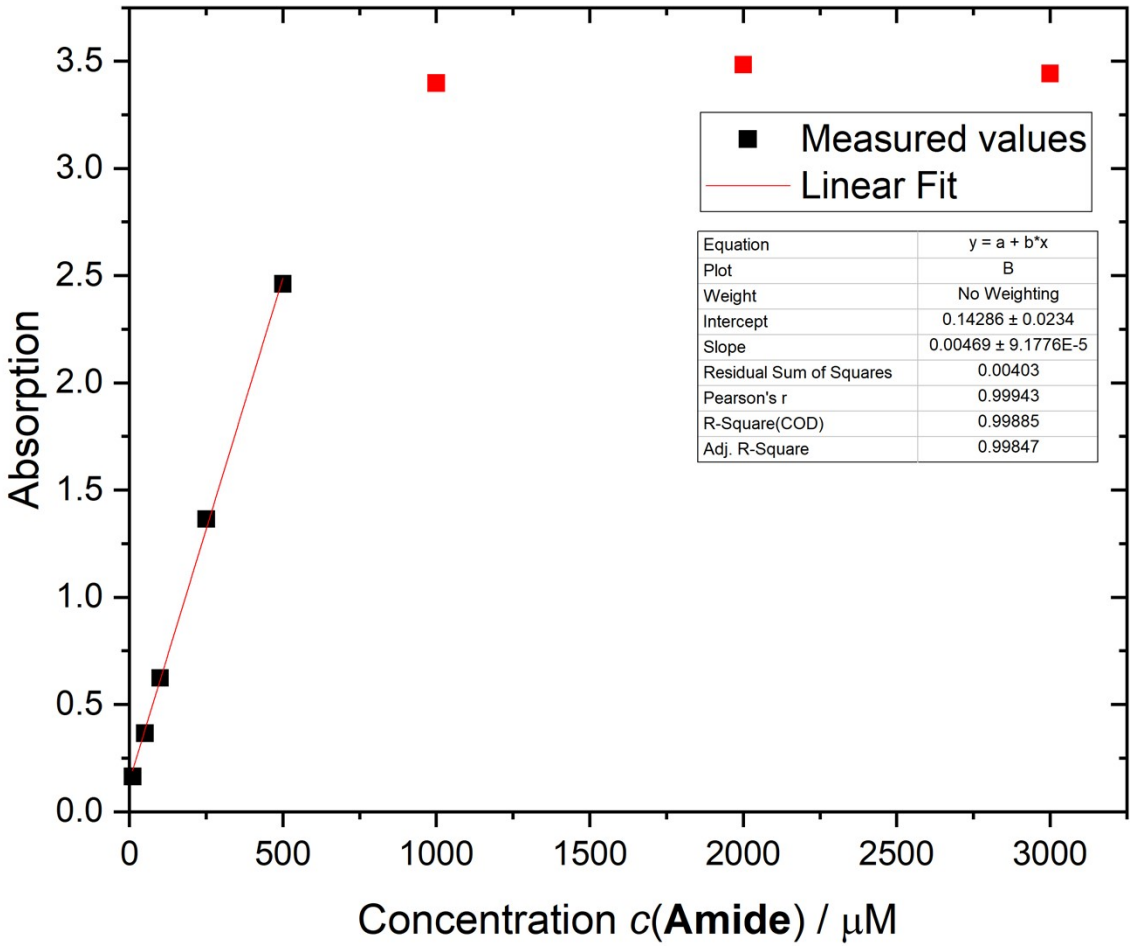

Figure S17. Calibration curve for the 4-nitroaniline concentration in the assay mixture.

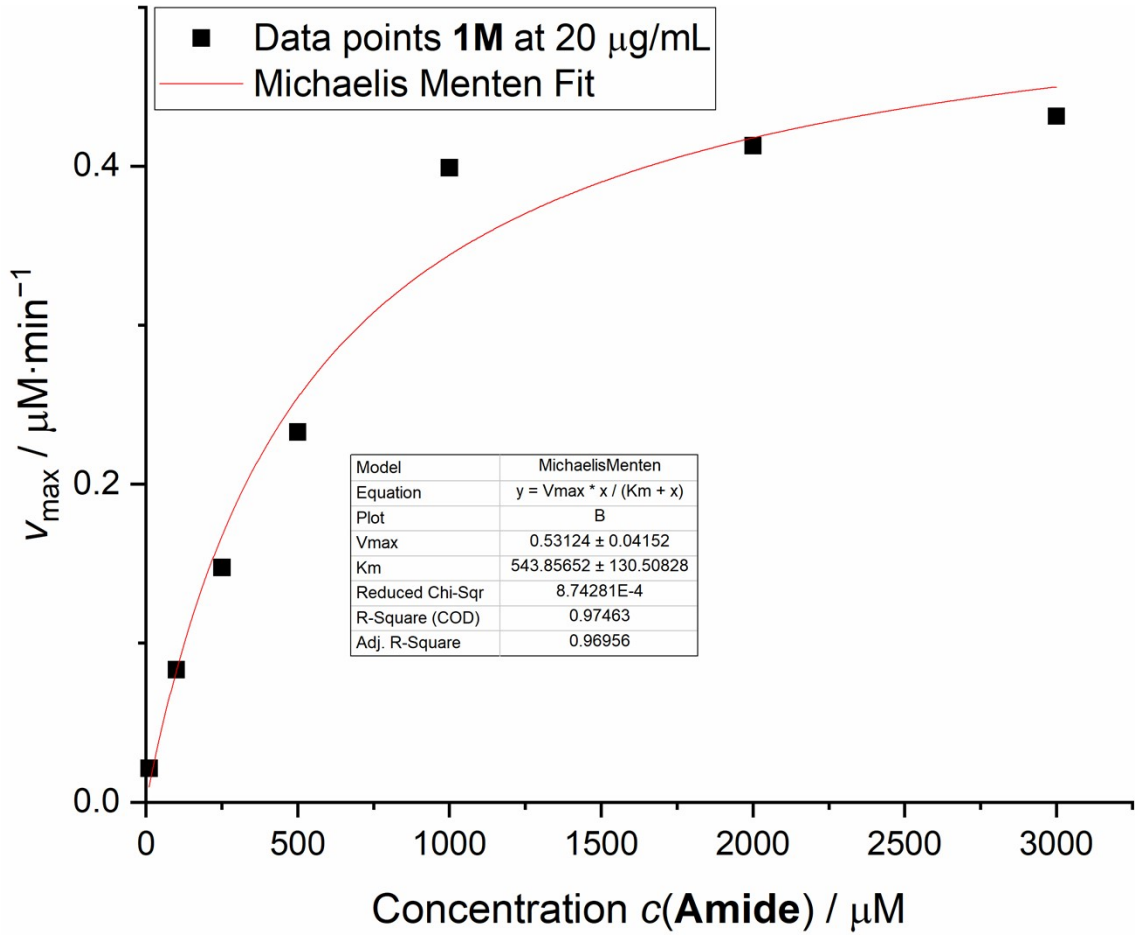

Figure S18. Michaelis–Menten plot for Bs2 F398D, run 1.

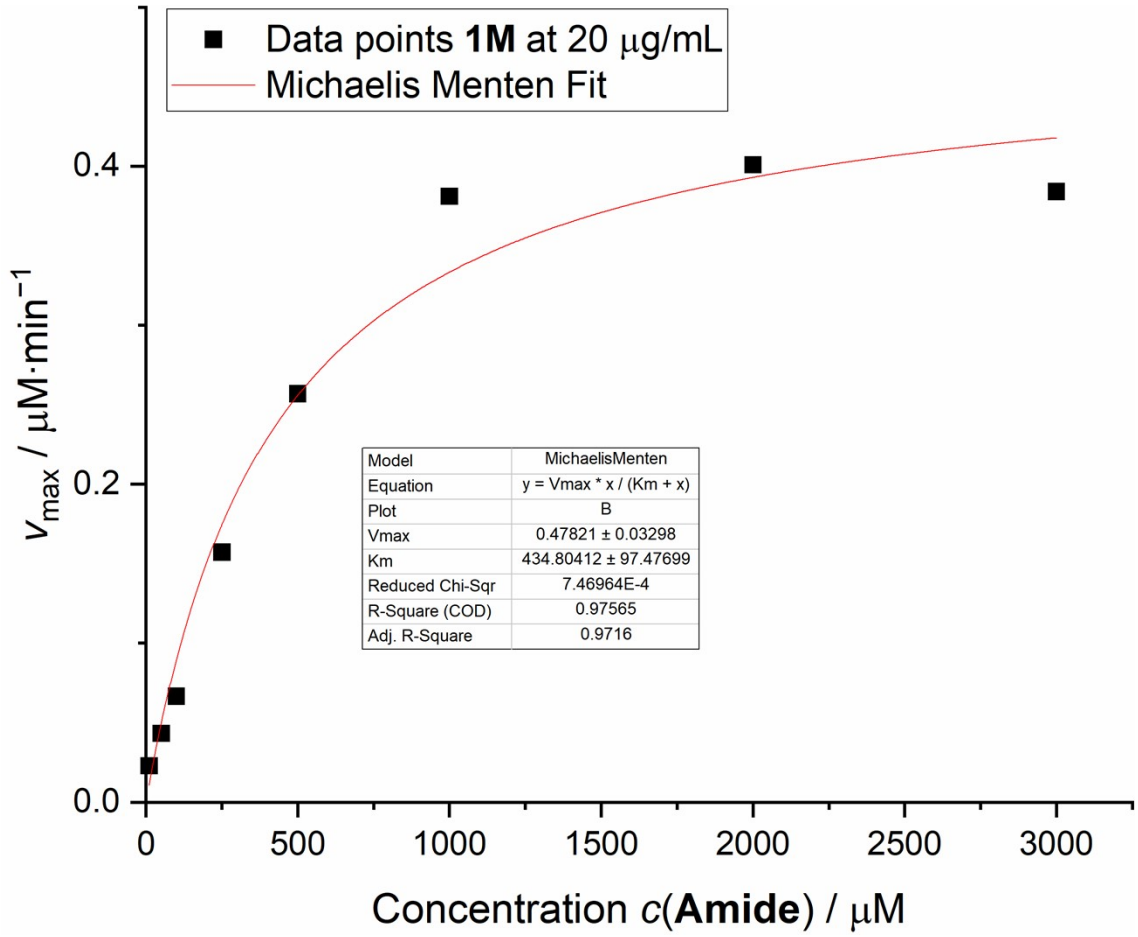

Figure S19. Michaelis–Menten plot for Bs2 F398D, run 2.

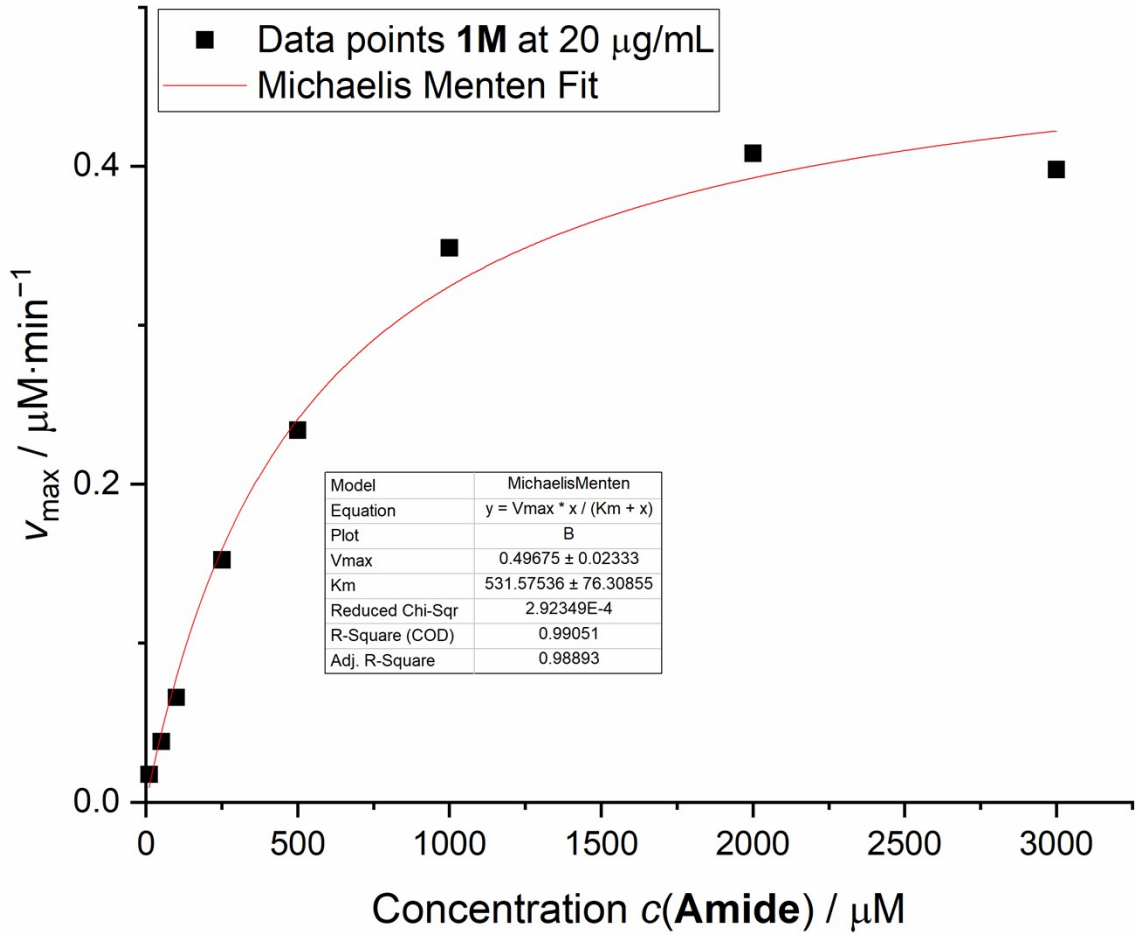

Figure S20. Michaelis–Menten plot for Bs2 F398D, run 3.

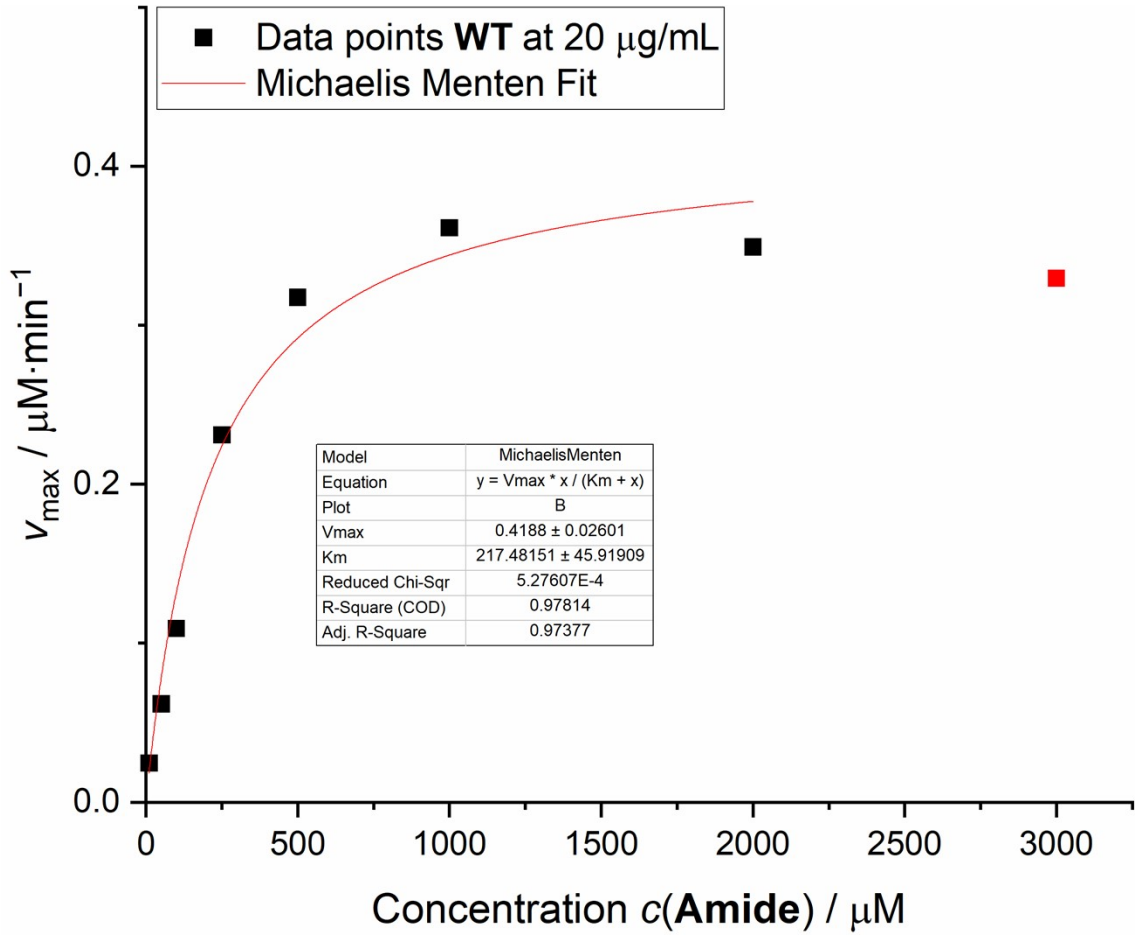

Figure S21. Michaelis–Menten plot for wild-type Bs2, run 1. Red data point was not included in fit.

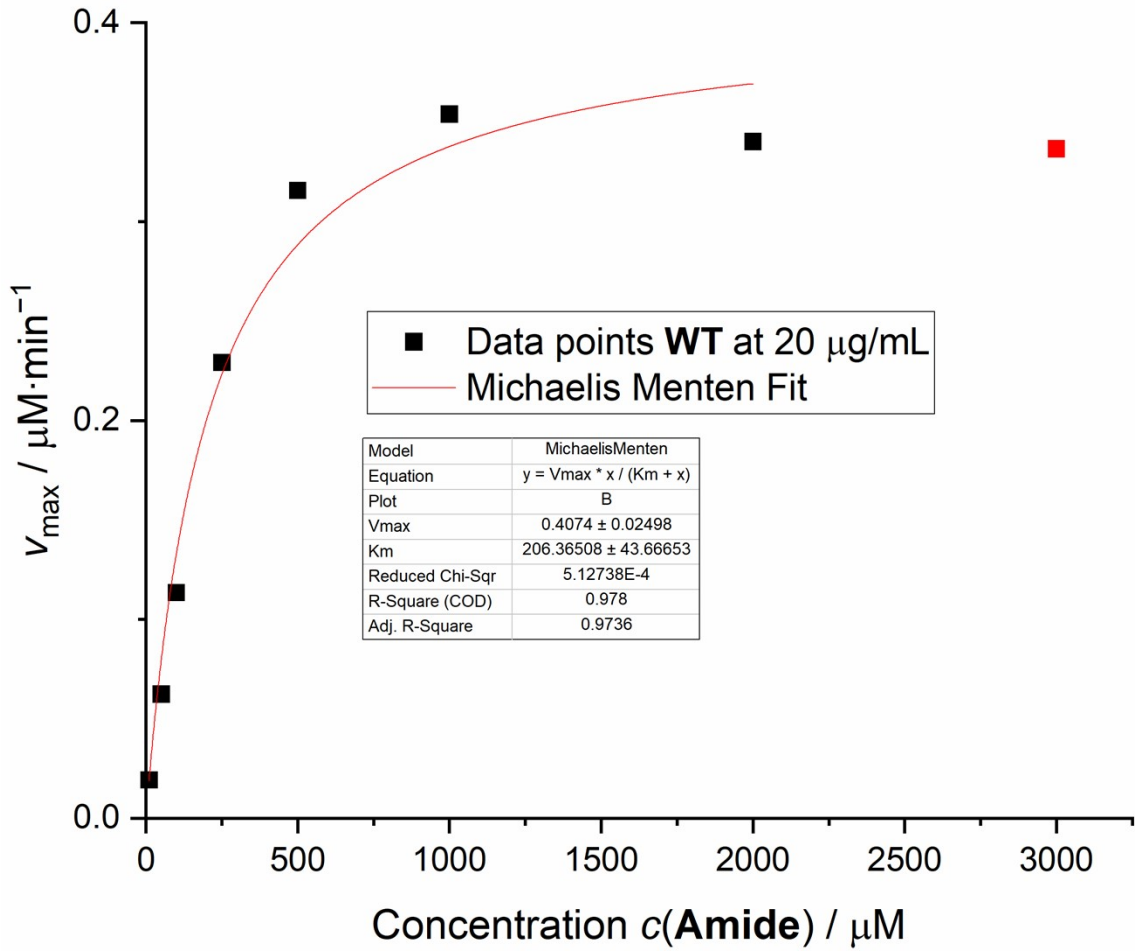

Figure S22. Michaelis–Menten plot for wild-type Bs2, run 2. Red data point was not included in fit.

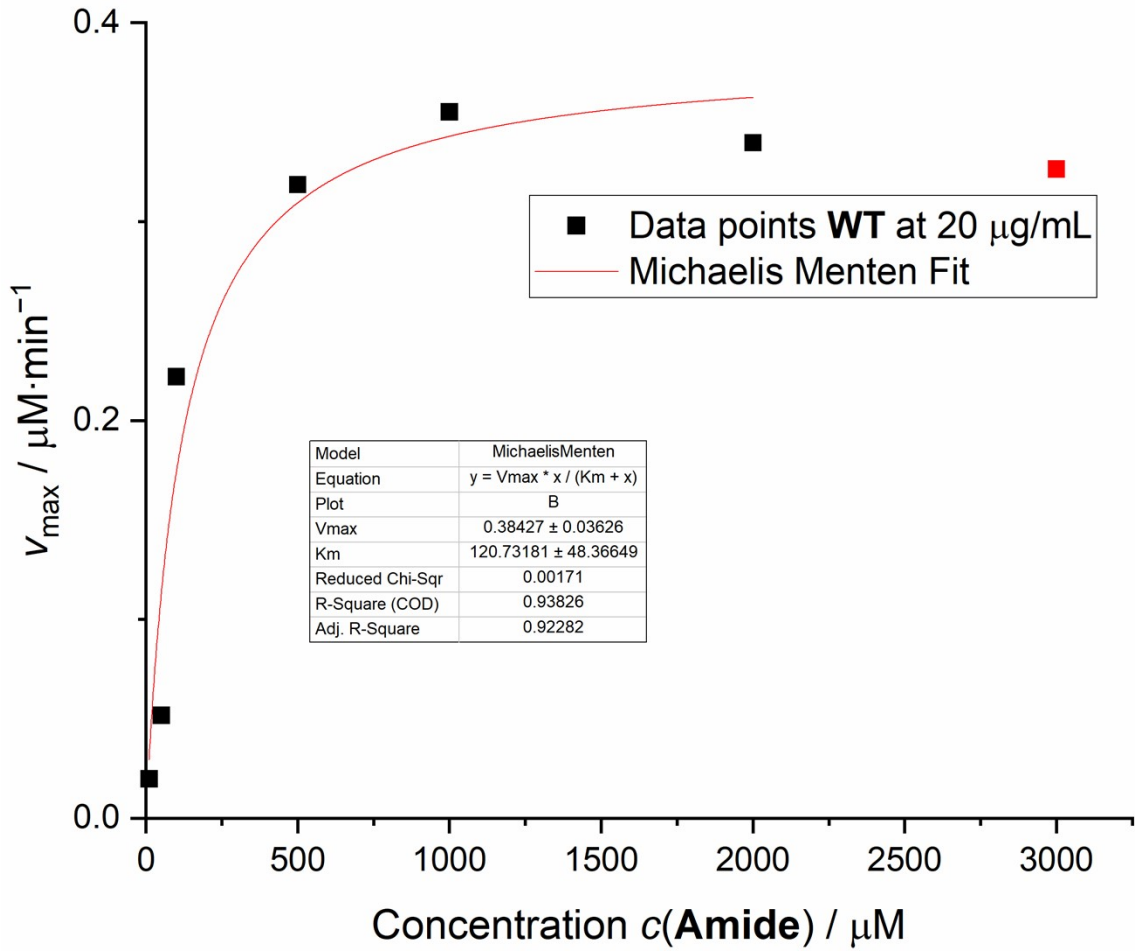

Figure S23. Michaelis–Menten plot for wild-type Bs2, run 3. Red data point was not included in fit.

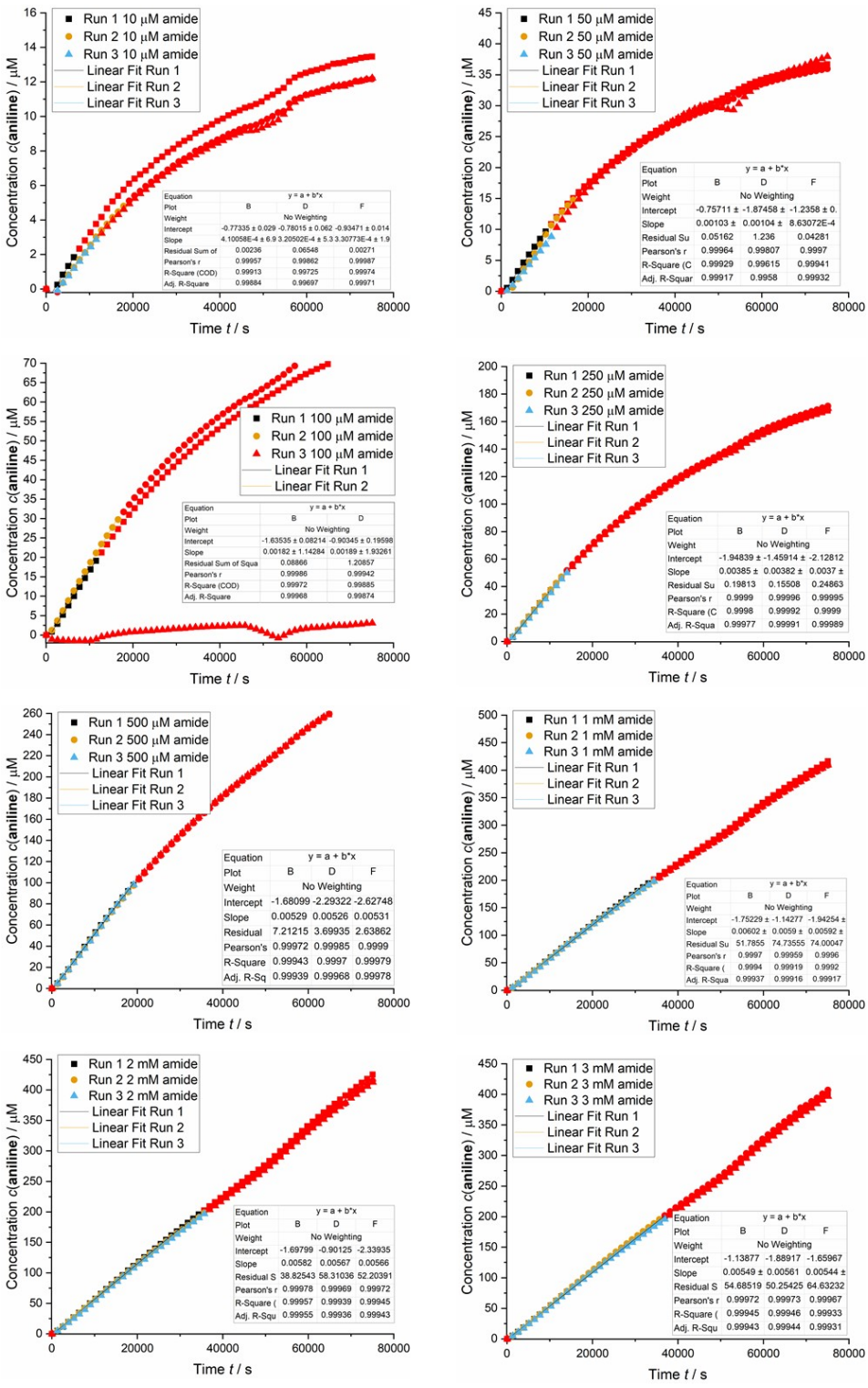

Figure S24. Kinetic profiles for wild-type Bs2. Red data points were not included for the fit for being out of the linear range.

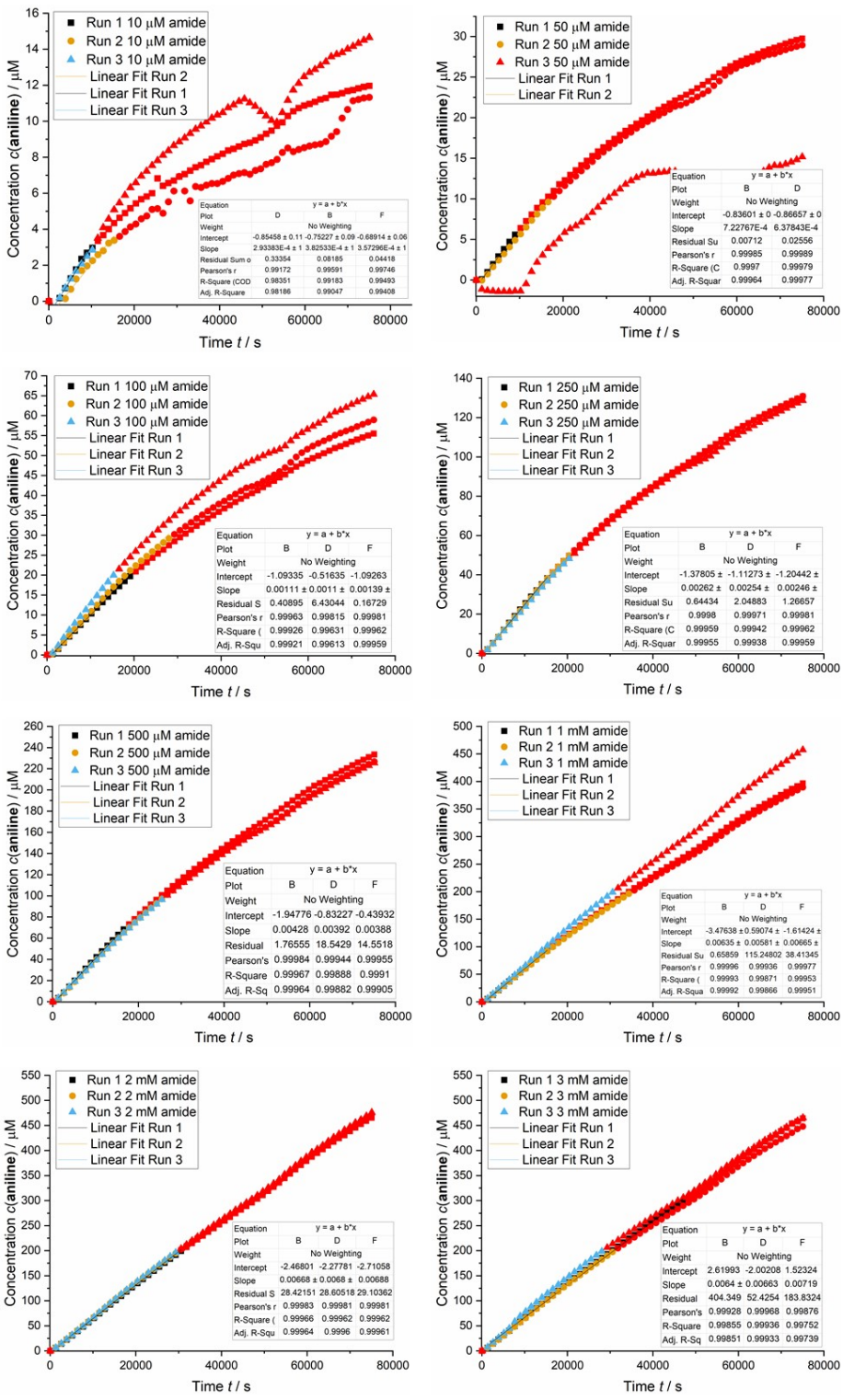

Figure S25. Kinetic profiles for Bs2 F398D. Red data points were not included for the fit for being out of the linear range.

Table S11. Exact kinetic values obtained from fitting software and derived from assay triplicates (Figures S18-S25). Values are means with population standard deviation given.

	wild-type Bs2	Bs2 F398D
v_{max} / μM min^{-1}	0.40349 ± 0.014365	0.502067 ± 0.021973
k_{cat} / min^{-1}	1.112422 ± 0.039605	1.383394 ± 0.060546
K_M / μM^{-1} min^{-1}	181.5261 ± 43.22697	503.412 ± 48.77149

REFERENCES

(1) Hackenschmidt, S.; Moldenhauer, E. J.; Behrens, G. A.; Gand, M.; Pavlidis, I. V.; Bornscheuer, U. T. Enhancement of Promiscuous Amidase Activity of a Bacillus Subtilis Esterase by Formation of a π-π Network. *ChemCatChem* **2014**, *6*, 1015–1020.

(2) Consortium, T. U. UniProt: A Worldwide Hub of Protein Knowledge. *Nucleic Acids Res.* **2018**, *47*, D506–D515.

(3) Spiller, B.; Gershenson, A.; Arnold, F. H.; Stevens, R. C. A Structural View of Evolutionary Divergence. *Proc. Natl. Acad. Sci.* **1999**, *96*, 12305–12310.

(4) Sali, A.; Blundell, T. L. Comparative Protein Modelling by Satisfaction of Spatial Restraints. *J. Mol. Biol.* **1993**, *234*, 779–815.

(5) Galmés, M. À.; Nödling, A. R.; Luk, L.; Świderek, K.; Moliner, V. Combined Theoretical and Experimental Study to Unravel the Differences in Promiscuous Amidase Activity of Two Nonhomologous Enzymes. *ACS Catal.* **2021**, 8635–8644.

(6) Olsson, M. H. M.; SØndergaard, C. R.; Rostkowski, M.; Jensen, J. H. PROPKA3: Consistent Treatment of Internal and Surface Residues in Empirical p Kapredictions. *J. Chem. Theory Comput.* **2011**, *7*, 525–537.

(7) Søndergaard, C. R.; Olsson, M. H. M.; Rostkowski, M.; Jensen, J. H. Improved Treatment of Ligands and Coupling Effects in Empirical Calculation and Rationalization of PKa Values. *J Chem Theory Comput* **2011**, *7*, 2284–2295.

(8) Jorgensen, W. L.; Chandrasekhar, J.; Madura, J. D.; Impey, R. W.; Klein, M. L. Comparison of Simple Potential Functions for Simulating Liquid Water. *J. Chem. Phys.* **1983**, *79*, 926–935.

(9) Galmés, M. A.; García-Junceda, E.; Świderek, K.; Moliner, V. Exploring the Origin of Amidase Substrate Promiscuity in CALB by a Computational Approach. *ACS Catal.* **2020**, *10*, 1938–1946.

(10) Duan, Y.; Wu, C.; Chowdhury, S.; Lee, M. C.; Xiong, G.; Zhang, W. E. I.; Yang, R.; Cieplak, P.; Luo, R. A. Y.; Lee, T.; Caldwell, J.; Wang, J.; Kollman, P. A Point-Charge Force Field for Molecular Mechanics Simulations of Proteins Based on Condensed-Phase. *J. Comput. Chem.* **2003**, *24*, 1999–2012.

(11) Phillips, J. C.; Braun, R.; Wang, W. E. I.; Gumbart, J.; Tajkhorshid, E.; Villa, E.; Chipot, C.;

Skeel, R. D.; Poincare, H. Scalable Molecular Dynamics with NAMD. *J. Comput. Chem.* **2005**, *26*, 1781–1802.

(12) Grest, G. S.; Kremer, K. Molecular Dynamics Simulation for Polymers in the Presence of a Heat Bath. *Phys. Rev. A* **1986**, *33*, 3628–3631.

(13) Case, D. A.; Aktulga, H. M.; Belfon, K.; Ben-Shalom, I. Y.; Brozell, S. R.; Cerutti, D. S.; Cheatham, T. E. I. I. I.; Cruzeiro, V. W. D.; Darden, T. A.; Duke, R. E.; Giambasu, G.; Gilson, M. K.; Gohlke, H.; Goetz, A. W.; Harris, R.; Izadi, S.; Izmailov, S. A.; Jin, C.; Kasavajhala, K.; et al. Amber 2021. University of California: San Francisco 2021.

(14) Field, M. J.; Bash, P. A.; Karplus, M. A Combined Quantum Mechanical and Molecular Mechanical Potential for Molecular Dynamics Simulations. *J. Comput. Chem.* **1990**, *11*, 700–733.

(15) Jorgensen, W. L.; Maxwell, D. S.; Tirado-Rives, J. Development and Testing of the OPLS All-Atom Force Field on Conformational Energetics and Properties of Organic Liquids. *J. Am. Chem. Soc.* **1996**, *118*, 11225–11236.

(16) Field, M. J.; Albe, M.; Bret, C.; Proust-De Martin, F.; Thomas, A. The Dynamo Library for Molecular Simulations Using Hybrid Quantum Mechanical and Molecular Mechanical Potentials. *J. Comput. Chem.* **2000**, *21*, 1088–1100.

(17) Dewar, M. J. S.; Zoebisch, E. G.; Healy, E. F.; Stewart, J. J. P. Development and Use of Quantum Mechanical Molecular Models. 76. AM1: A New General Purpose Quantum Mechanical Molecular Model. *J. Am. Chem. Soc.* **1985**, *107*, 3902–3909.

(18) Zhao, Y.; Truhlar, D. G. The M06 Suite of Density Functionals for Main Group Thermochemistry, Thermochemical Kinetics, Noncovalent Interactions, Excited States, and Transition Elements: Two New Functionals and Systematic Testing of Four M06-Class Functionals and 12 Other Function. *Theor. Chem. Acc.* **2008**, *120*, 215–241.

(19) Stewart, J. J. P. Quantum Chemistry Program Exchange 455. **1996**, *6*.

(20) Frisch, M. J.; Trucks, G. W.; Schlegel, H. B.; Scuseria, G. E.; Robb, M. A.; Cheeseman, J. R.; Scalmani, G.; Barone, V.; Petersson, G. A.; Nakatsuji, H.; Li, X.; Caricato, M.; Marenich, A. V; Bloino, J.; Janesko, B. G.; Gomperts, R.; Mennucci, B.; Hratchian, H. P.; Ortiz, J. V; et al. Gaussian 09, Revision E.01. Gaussian, Inc.: Wallingford, CT 2009.

(21) Byrd, R. H.; Lu, P.; Nocedal, J.; Zhu, C. A Limited Memory Algorithm for Bound Constrained Optimization. *SIAM J. Sci. Comput.* **1995**, *16*, 1190–1208.

(22) J. Turner, A.; Moliner, V.; H. Williams, I. Transition-State Structural Refinement with GRACE and CHARMM: Flexible QM/MM Modelling for Lactate Dehydrogenase. *Phys. Chem. Chem. Phys.* **1999**, *1*, 1323–1331.

(23) Martí, S.; Moliner, V.; Tuñón, I. Improving the QM/MM Description of Chemical Processes: A Dual Level Strategy to Explore the Potential Energy Surface in Very Large Systems. *J. Chem. Theory Comput.* **2005**, *1*, 1008–1016.

(24) Baker, J.; Kessi, A.; Delley, B. The Generation and Use of Delocalized Internal Coordinates in Geometry Optimization. *J. Chem. Phys.* **1996**, *105*, 192–212.

(25) Baker, J. Constrained Optimization in Delocalized Internal Coordinates. *J. Comput. Chem.* **1997**, *18*, 1079–1095.

(26) Roux, B. The Calculation of the Potential of Mean Force Using Computer-Simulation. *Comput. Phys. Commun.* **1995**, *91*, 275–282.

(27) Torrie, G. M.; Valleau, J. P. Non-Physical Sampling Distibutions in Monte-Carlo Free-Energy Estimation - Umbrella Sampling. *J. Comput. Phys.* **1977**, *23*, 187–199.

(28) Kumar, S.; Rosenberg, J. M.; Bouzida, D.; Swendsen, R. H.; Kollman, P. A. The Weighted Histogram Analysis Method for Free-energy Calculations on Biomolecules. I. The Method. *J. Comput. Chem.* **1992**, *13*, 1011–1021.

(29) Verlet, L. Computer “Experiments” on Classical Fluids. I. Thermodynamical Properties of Lennard-Jones Molecules. *Phys. Rev.* **1967**, *159*, 98–103.

(30) Ruiz-Pernía, J. J.; Silla, E.; Tuñón, I.; Martí, S.; Moliner, V. Hybrid QM/MM Potentials of Mean Force with Interpolated Corrections. *J. Phys. Chem. B* **2004**, *108*, 8427–8433.

(31) Ruiz-Pernía, J. J.; Silla, E.; Tuñón, I.; Martí, S. Hybrid Quantum Mechanics/Molecular Mechanics Simulations with Two-Dimensional Interpolated Corrections: Application to Enzymatic Processes. *J. Phys. Chem. B* **2006**, *110*, 17663–17670.

(32) Martí, S. QMCube (QM3): An All-Purpose Suite for Multi Scale QM/MM Calculations.

(33) Kneller, G. R. Superposition of Molecular Structures Using Quaternions. *Mol. Simul.* **1991**, *7*,

113–119.